http://dx.doi.org/10.1038/nmicrobiol.2015.6

THPP target assignment reveals EchA6 as an essential fatty acid shuttle in mycobacteria

Jonathan A. G. Cox[1#], Katherine A. Abrahams[1#], Carlos Alemparte[2], Sonja Ghidelli-Disse[3], Joaquín Rullas[2], Iñigo Angulo-Barturen[2], Albel Singh[1], Sudagar S. Gurcha[1], Vijayashankar Nataraj[1], Stephen Bethell[1], Modesto J. Remuiñán[2], Lourdes Encinas[2], Peter J. Jervis[1], Nicholas C. Cammack[2], Apoorva Bhatt[1], Ulrich Kruse[3], Marcus Bantscheff[3], Klaus Fütterer[1*], David Barros[2], Lluis Ballell[2*], Gerard Drewes[3], Gurdyal S. Besra[1*]

[1]Institute of Microbiology and Infection, School of Biosciences, University of Birmingham, Edgbaston, Birmingham B15 2TT, UK, [2]Diseases of the Developing Word, GlaxoSmithKline, Severo Ochoa 2, 28760 Tres Cantos, Madrid, Spain, [3]Cellzome - a GSK Company, Meyerhofstrasse 1, 69117 Heidelberg, Germany

[#]These authors contributed equally to this work.

[*]E-mail for correspondence material requests: g.besra@bham.ac.uk (TEL: +00 44 121 415 8125; FAX +00 44 121 414 5925), Lluis.p.ballell@gsk.com (TEL: +34676861497), k.futterer@bham.ac.uk (TEL: +00 44 121 414 5895)

Key words: Tuberculosis, chemical proteomics, THPP, EchA6, drug discovery

Summary

Phenotypic screens for bactericidal compounds against drug-resistant tuberculosis are beginning to yield novel inhibitors. However, reliable target identification remains challenging. Here we show that tetrahydropyrazo[1,5-*a*]pyrimidine-3-carboxamide (THPP) selectively pulls down EchA6 in a stereospecific manner, instead of the previously assigned target *M. tuberculosis* MmpL3. While homologous to mammalian enoyl-CoA hydratases, EchA6 is non-catalytic yet essential, and binds long-chain acyl-CoAs. THPP inhibitors compete with CoA-binding, suppress mycolic acid synthesis and are bactericidal in a mouse model of chronic tuberculosis infection. A point mutation, W133A, abrogated THPP-binding and increased both the *in vitro* minimum inhibitory concentration and the *in vivo* effective-dose 99 in mice. Surprisingly, EchA6 interacts with selected enzymes of fatty acid synthase II (FAS-II) in bacterial two-hybrid assays, suggesting essentiality may be linked to feeding long-chain fatty acids to FAS-II. Finally, our data show that spontaneous resistance-conferring mutations can potentially obscure the actual target or alternative targets of small molecule inhibitors.

43 *Mycobacterium tuberculosis*, the causative agent of tuberculosis (TB), is a global
44 disease with an estimated 8.7 million new cases and around 1.4 million deaths
45 annually[1]. TB drug-resistance first emerged 40 years ago, but since then has grown to
46 an alarming level requiring the development of new antibiotics. Although enzyme-
47 screening campaigns have dominated antibiotic discovery for years, their lack of
48 success has prompted a change of strategy. In many instances, target identification of
49 phenotypic hits is initiated by generating spontaneous drug-resistant mutants, with the
50 expectation that resistance-conferring mutations will be revealed by whole genome
51 sequencing (WGS)[2-5]. For instance, Bedaquiline was identified as an inhibitor of the
52 *M. tuberculosis* F_0F_1 ATP synthase through WGS of spontaneous resistant mutants[6].
53 Using the same approach, MmpL3 was shown to be targeted by several inhibitors
54 including SQ109, adamantyl ureas, BM212, THPPs, SPIROs and NITDs[7-13].
55 However, spontaneous resistance can occur through mutations not only in the drug
56 target but also in other proteins linked to interactions between the cell and
57 inhibitor[14,15]. In this study, we were able to exploit stereoselectivity of ligand binding
58 in a quantitative affinity pull-down to identify the target of THPPs and reveal a novel
59 fatty acid shuttle in mycobacteria.
60
61 **Results**
62
63 **Target identification**
64
65 THPPs were prepared in a four-step synthetic route (**Fig. 1a**) and the desired
66 enantiomer separated by chiral-HPLC. GSK366A and GSK951A[12], and two novel
67 THPP analogues, GSK059A and GSK572A, were included as tool compounds for

68 mode of action and structural studies. All compounds were endowed with selective
69 anti-tubercular potency and were devoid of any significant cytotoxicity against
70 HepG2 cell lines (**Fig. 1b**). Compound GSK951A was progressed to a dose response
71 analysis in a murine model of chronic TB infection (**Fig. 1c**)[12]. Thus, GSK951A
72 combines potency in culture with *in vivo* activity and lack of cytotoxicity.
73
74 We applied a chemical proteomics strategy to identify the protein target(s) of the
75 THPP lead compound directly in *M. bovis* BCG extracts. To this end, we synthesized
76 carboxylic acid analogues of the active (GSK729) and inactive (GSK730) THPP
77 enantiomers suitable for immobilization to Sepharose beads (**Fig. 2**). Each type of
78 bead was incubated with *M. bovis* BCG extracts under three different conditions: (i)
79 in presence of vehicle, (ii) in presence of excess "free" active enantiomer analogue,
80 and (iii) in presence of excess "free" inactive enantiomer analogue. The relative
81 protein content captured by the beads from each sample was quantified by isobaric
82 tagging of tryptic peptides and tandem mass spectrometry analysis of the combined
83 peptide pools in a 6-plex format[16]. Target proteins would be expected to bind
84 selectively to beads derivatized with the active enantiomer analogue, a preference we
85 probed by competition with free active *vs* free inactive enantiomers. Relative
86 quantification (**Supplementary Table 1** and **2**) demonstrated that only a single
87 protein showed a pronounced preference in this competition assay. The putative
88 enoyl-CoA hydratase EchA6 showed robust inhibition (92%) by the active
89 enantiomer GSK729 to the binding of GSK729-derived beads, but only insignificant
90 inhibition (16%) by its inactive enantiomer GSK730 (**Fig. 2a,b**). MmpL3 was readily
91 detected within the whole proteome analysis of the *M. bovis* BCG extract, but it was
92 not identified in pull-downs with the immobilized THPP analogues. This does not

93 necessarily rule it out as a target, since it could be due to either steric hindrance by the
94 linker on the compound, low affinity, or denaturation of the extracted MmpL3.
95 Supporting the specificity of the GSK729-beads, in similar experiments performed
96 with HepG2 cells, the beads did not capture the closest human EchA6 orthologue,
97 ECH1. To determine the affinity of GSK729 for EchA6 in *M. bovis* BCG extracts, we
98 optimized the concentration of immobilized ligands on the beads, enabling a dose-
99 dependent binding of EchA6 to GSK729 in *M. bovis* BCG extracts with an IC_{50} of 1.8
100 μM (**Fig. 2c** and **Supplementary Table 2** and **3**).
101
102 ***EchA6* is essential and GSK951A inhibits mycolic acid biosynthesis**
103
104 To confirm essentiality we used a genetic tool termed CESTET[17,18]. Initially, a
105 merodiploid strain in *M. bovis* BCG was generated that contained a second integrated
106 copy of *echA6* (*Rv0905*) under the control of the inducible tetracycline (ATc)
107 promoter and subsequently the genomic copy was disrupted. As shown in
108 **Supplementary Figure 1a,** the strain grew normally in liquid medium with ATc, but
109 eventually showed cell lysis when grown in medium lacking ATc (**Supplementary**
110 **Fig. 1a, inset)**. To evaluate the effect of depletion of *echA6* on both mycolic acid and
111 fatty acid synthesis in *M. bovis* BCG, mycolic acid methyl esters (MAMES) and fatty
112 acid methyl esters (FAMES) were prepared from cultures following labeling with
113 [^{14}C]-acetate. As shown in **Supplementary Figure 1b**, conditional depletion of
114 *echA6* results in a reduction of α-MAMES and keto-MAMES, while the overall
115 abundance of FAMES remains largely unaffected, a classic hallmark of inhibitors
116 targeting mycolic acid biosynthesis[14,19].
117

118 In light of these findings we decided to further investigate our previous studies on the
119 effects of THPPs on mycolic acid synthesis[12]. As shown in **Figure 3a left panel**,
120 GSK951A suppresses the synthesis of all classes of MAMES in *M. bovis* BCG, while
121 the overall abundance of FAMES remains largely unaffected. This result is similar to
122 the mode of action of the thiolactomycin (TLM) and INH, well-known inhibitors of
123 mycolic acid biosynthesis[14,19] **(Fig. 3a, right panel**), supporting our earlier *echA6*
124 conditional depletion experiments (**Supplementary Fig. 1b**). Further resolution of the
125 FAMES by reverse-phase TLC indicated the accumulation of C26 FAMES (**Fig. 3b**),
126 suggesting that THPPs act downstream of fatty acid synthase-I (FAS-I), and similar to
127 the mode of action of INH (**Fig. 3a**,**f**). In addition, GSK951A significantly suppressed
128 the synthesis of cell wall bound MAMES (**Fig. 3a, middle panel**). In marked
129 contrast, using the inactive enantiomer, GSK540A, even at a minimum inhibitor
130 concentration (MIC) of 20 × that of GSK951A, failed to inhibit total
131 MAMES/FAMES and cell wall bound MAMES (**Supplementary Fig. 2**). Whole-cell
132 target engagement of GSK951A was supported by increased resistance when *echA6*
133 was overexpressed in *M. bovis* BCG. *M. tuberculosis echA6* (*Rv0905*) was cloned into
134 the multi-copy plasmid pVV16, which resulted in overexpression of His-tagged
135 EchA6 as shown by Western Blot analysis (**Fig. 3c**). Upon labeling cultures with
136 [^{14}C]-acetate, pVV16-*echA6* containing strains revealed an elevated synthesis of
137 MAMES (**Supplementary Fig. 1c left panel**, and **d**) and a 6-fold increased-resistance
138 to GSK951A with solid or liquid media (MIC of 1.60 - 2.00 μM), in comparison to
139 the pVV16 vector control strain (MIC of 0.32 μM) (**Supplementary Fig. 1e** and **Fig.**
140 **3d**). Finally, the synthesis of cell wall bound MAMES in the pVV16-*echA6* strain was
141 less refractory to the addition of GSK951A at 1 × MIC compared to the pVV16 vector
142 control strain (**Supplementary Fig. 1c, right panel**).

143

144 The addition of GSK951A to cultures up to 4 × the MIC resulted in no significant
145 difference in terms of extractable cell envelope lipids (**Supplementary Fig. 3, Panels**
146 **A-C**). The organic solvent extractable mycolates were markedly altered in the
147 presence of GSK951A, and overall resulted in an elevated level of TMM
148 (**Supplementary Fig. 3**, **Panels D1** and **D2**). Indeed, confirmed MmpL3 inhibitors,
149 including SQ109 and BM212, have been reported to cause significant accumulation
150 of TMM[13]. Nevertheless, when applied at concentrations of up to 4 × their respective
151 MICs, SQ109 or BM212 had no effect on total MAMES, and only moderately
152 inhibited cell wall bound MAMES (**Supplementary Fig. 2**). In contrast, GSK951A
153 effectively suppressed both total and cell wall bound MAMES at concentrations well
154 below the 4 × MIC margin, emphasising the distinctive phenotypic response of
155 GSK951A. Interestingly, we have observed an increased sensitivity to GSK951A
156 when MmpL3 (Rv0206c) was overexpressed in *M. bovis* BCG using the multi-copy
157 plasmid pMV261-*mmpL3*, in comparison to the pMV261 vector control
158 (**Supplementary Fig. 1f**). Increased sensitivity to GSK951A would be consistent
159 with MmpL3 moonlighting as a THPP importer, in addition to its function as a TMM
160 exporter. Taken together, these findings provide strong evidence for THPPs acting
161 upstream of fatty acid synthase-II (FAS-II) (**Fig. 3f**), without excluding the possibility
162 of a downstream activity *via* MmpL3. To further probe the possible interaction of
163 EchA6 with components of FAS-II, we conducted a protein-protein interaction screen
164 using the bacterial two-hybrid system-BACTH. Interestingly, we found preliminary
165 evidence for EchA6 interacting with two specific components of FAS-II (**Fig. 3e**,**f**).
166 These included the β-ketoacyl-ACP synthase KasA, and the enoyl-ACP reductase

167 InhA (**Fig. 3e**). No interactions were observed with other specific components of the
168 core multi-enzyme FAS-II complex[20].
169
170 **Acyl-CoA and THPP ligand binding**
171
172 Initial inspection of the sequence of EchA6 and related family members from *M.*
173 *tuberculosis* indicated that the conserved carboxylate side chains[21] were mutated in
174 EchA6, suggesting that EchA6, despite resembling an enoyl-CoA hydratase in overall
175 sequence, was inactive. Nevertheless, residues involved in binding CoA are partially
176 conserved in EchA6, leaving open the possibility that binding of acyl-CoAs was
177 preserved, possibly as a mechanism for providing long-chain acyl-CoAs for fatty acid
178 biosynthesis *via* FAS-II. Using intrinsic tryptophan fluorescence (ITF), we assayed
179 variable chain-length acyl-CoA binding, which indicated that EchA6 has a clear
180 preference for acyl-CoAs of chain-lengths 12 carbons or greater (**Supplementary**
181 **Table 4** and **Fig. 4a**). Ligand binding assays using EchA6 and THPPs were conducted
182 to establish K_d values for a selection of compounds (**Supplementary Table 4**),
183 highlighting that GSK951A (**Fig. 4b**) and GSK572A bound with the highest affinity
184 as reflected by K_d values of 0.45 μM and 1.9 μM, respectively. In contrast,
185 GSK573A, which is the inactive enantiomer of GSK572A, bound with a K_d of 285.8
186 μM, a 150-fold increase, underscoring the distinct stereospecificity of the interaction
187 between THPP compounds and EchA6 (**Supplementary Table 4**). Assessing C_{20}-
188 CoA binding following pre-incubation of EchA6 with GSK951A, at concentrations of
189 0.25 μM, 2.5 μM, and 10 μM of the drug, resulted in a distinct weakening of the
190 interaction with C_{20}-CoA, thus indicating competition for the same binding site (**Fig.**
191 **4c**). Similar experiments with C_4-CoA (**Fig. 4d**) indicated that competition between

192 acyl-CoA and GSK951A for the EchA6 binding site was not solely dependent on the
193 acyl-chain. While C_4-CoA bound with less affinity than C_{20}-CoA, the K_d increased by
194 similar margins when competing with GSK951A (**Supplementary Table 4**).
195 However, the increase was monotonic for C_4-CoA, while raising GSK951A above 2.5
196 μM did not result in a further increase of K_d for binding of C_{20}-CoA. Finally,
197 introducing the point mutation, W133A, which maps to the THPP binding site (see
198 **Fig. 6**), completely abolished THPP binding (**Fig. 4b**), whilst C_{20}-CoA binding was
199 weakened, but not abrogated (**Supplementary Table 4**).
200
201 ***In vivo* target engagement of THPPs and EchA6**
202
203 In an acute TB infection model[22], *M. tuberculosis* transformed with a multi-copy
204 plasmid-borne *echA6*^{W133A} resulted in a significant shift in the *in vivo* effective dose
205 99 (ED_{99}) of GSK951A when compared to strains transformed with empty vector or
206 vector containing *echA6*. (**Fig. 1d**). The *echA6*^{W133A} strain resulted in a significant
207 increase in the ED_{99} of GSK951A, from 85 and 77 mg/kg for the empty vector and
208 *echA6* strains, to >250 mg/kg for the *echA6*^{W133A} strain (**Fig. 1d, right panel**). This
209 increase of ED_{99} was well outside the calculated 95 % confidence interval (CI) for the
210 empty vector and *echA6* strains (41-182 mg/kg). As a control, all strains possessed
211 similar ED_{99} values for INH (**Fig. 1d, left panel**) and were within the calculated 95 %
212 CI range (0.2-3 mg/kg). While the empty vector and *echA6* strains were able to grow
213 at the same rate when inoculated into C57BL/6 mice in the acute TB infection model,
214 the *echA6*^{W133A} strain was relatively attenuated for growth (**Fig. 1e**), suggesting that
215 the viability of *M. tuberculosis in vivo* was compromised by the EchA6 point
216 mutation that weakened acyl-CoA binding. In addition, *M. bovis* BCG transformed

217 with a multi-copy plasmid-borne *echA6*^{W133A} and grown in broth, showed a further
218 increased resistance to GSK951A, possessing a MIC of 3.20 μM. This is in
219 comparison to a *M. bovis* BCG strain transformed with plasmid-borne *echA6*
220 possessing a MIC of 1.60 μM. Complete abrogation of THPP binding by EchA6^{W133A}
221 would suggest a more pronounced effect, however, the wild-type copy present in the
222 overexpressing strain could account for the modest MIC and ED_{99} increase.
223
224 **X-ray crystallographic analysis of EchA6**
225
226 X-ray crystallographic structures of EchA6 in the ligand-free form, bound to C_{20}-CoA
227 and several THPPs were determined by molecular replacement (**Supplementary**
228 **Table 5**). EchA6 (**Fig. 5a**) consistently crystallized as a trimer (**Fig. 5b**), structurally
229 resembling a flat disk with 3 extended substrate-binding grooves (**Fig. 5c**). The
230 binding sites of the CoA-moiety and the THPPs reside on the 'front' and 'back' faces
231 of the trimer, respectively (**Fig. 5c**).
232
233 The EchA6 monomer is structurally similar to the rat liver enoyl-CoA hydratase
234 (RnECH)[23] (**Fig. 5a,b** and **Supplementary Fig. 4a**). However, the C-terminal helices
235 α10 and α11 diverge from the orientation seen in RnECH (**Supplementary Fig. 4a**).
236 In RnECH, the backbone turns 180º after helix α9 and helix α10 runs anti-parallel to
237 α9, whereas in EchA6, helices α10 and α11 project forward and fold back onto the
238 monomer (**Fig. 5a**). Despite the altered backbone conformation, helices α10 and α11
239 still occupy analogous interfacial positions between the monomers in the context of
240 the trimer (**Fig. 5b**).
241

242 Enoyl-CoA hydratases belong to the crotonase superfamily of enzymes, which display
243 diverse structural scaffolds and catalyze a wide variety of reactions, involving CoA-
244 linked substrates[24]. Among structural neighbours identified by distance matrix
245 alignment (DALI)[25], EchA6 aligns most closely with crotonases mediating enoyl-
246 CoA hydratase activity (e.g. RnECH, **Supplementary Fig. 4a**), in line with its
247 annotation in sequence databases. Yet, the catalytic residues are not conserved in
248 EchA6. The hydratase reaction converts the C2-C3 double bond of enoyl-CoA into a
249 single bond and adds a hydroxyl to C3. Polarization is facilitated by positioning the
250 acyl-keto oxygen against the amide nitrogens of nearby glycine and alanine residues
251 (Gly141, Ala98 in RnECH), while two carboxylate side chains (Glu144, Glu164 in
252 RnECH) coordinate the attacking water[21,23] (**Fig. 5d**). Comparing the structures of
253 EchA6 and RnECH (30.8% sequence identity), the oxyanion hole backbone amides
254 are conserved (Ala100, Ala60), but the carboxylate side chains are substituted by
255 glutamine (Gln103 for Glu144 of RnECH) and threonine (Thr123 for Glu164 of
256 RnECH), respectively (**Fig. 5d**). In contrast, the structural alignment of RnECH with
257 *M. tuberculosis* EchA8 (PDB entry 3PZK, 50.2 % identity) demonstrates complete
258 conservation of key residues in the active site (**Supplementary Fig. 4b**).
259 Nevertheless, the C_{20}-CoA bound complex of EchA6 (**Supplementary Fig. 4c**)
260 demonstrates a conserved mode of CoA-binding, with the thioester superimposing
261 closely with the thioesters in the acetoacetyl-CoA bound complexes of RnECH (PDB
262 entry 1EY3,[21]) and EchA8 (PDB entry 3Q0J). In addition, binding C_{20}-CoA to EchA6
263 induces a conformational change in the β3-α3 loop (residues 61-68), transforming the
264 substrate-binding groove into a tunnel between the 'front' and the 'back' face of the
265 EchA6 trimer (green subunit in **Fig. 5c**).
266

267 In order to define the structural determinants of THPP inhibition, we solved structures
268 of EchA6 in complex with five different THPPs (**Supplementary Table 5**, **Fig. 6a**,
269 and **Supplementary Fig. 4d-h**), including the lead compound GSK951A (**Fig. 1a**). In
270 the trimeric molecule, all 3 subunits are occupied by the ligand. Superposition of
271 ligand-bound and *apo* structures reveal only minor conformational adjustments of
272 side chains contacting the ligand. Situated on the 'back' face of the EchA6 trimer
273 (**Fig. 5c**), the inhibitor-binding site overlaps partially with the putative active site of
274 EchA6 (marked by the conserved oxyanion hole of Ala100 and Ala60), but mostly
275 occupies the extended hydrophobic groove, which accommodates the acyl-chain in
276 the C_{20}-CoA complex (**Fig. 5c** and **Fig. 6b**). The mode of binding is consistent
277 between all THPP-complexed structures (**Supplementary Table 5** and
278 **Supplementary Fig. 4d–h**). A slightly different ligand conformation is observed for
279 GSK366A (**Supplementary Fig. 4f**), but the difference could be the result of
280 different crystal symmetries (**Supplementary Table 5**), due to packing-induced
281 structural changes of the protein. The complex with the bait compound, GSK729A,
282 matches the binding mode of the other complexes (**Supplementary Fig. 4h**).
283 Interactions with EchA6 are dominated by hydrophobic and van der Waals (vdW)
284 contacts. The pyrazolo-pyrimidine group is central to the interaction with the protein.
285 The trifluoromethyl-substituent forms hydrogen bonds with His79 (to Nε2) and
286 Gln103 (to Oε1 and Nε2), with an additional vdW contact to Ile76 (Cδ1) (**Fig. 6c**).
287 The ethylphenyl group forms hydrophobic contacts with Trp133, the β-carbon of
288 Asp83 and the δ-carbon of Gln107 (**Fig. 6c**). For GSK951A, the terminal benzodioxol
289 group stacks on top of Phe216, with additional vdW contacts with the α-carbon of
290 Lys213 and the β-carbon of Ala208.
291

292 **Discussion**

293

294 Target identification by stereoselective quantitative pull-downs points to EchA6 as
295 the target of THPPs and is supported by a string of orthogonal evidence. This is in
296 contrast to the recent target assignment of THPPs as MmpL3[12], exposing an inherent
297 weakness of target identification by WGS of THPP-resistant mutants. Resistance-
298 conferring mutations against THPPs have not yet been observed in *echA6*, however,
299 our targeted mutagenesis studies have induced resistance, which strongly supports
300 THPPs acting through EchA6. The absence of SNPs in *echA6* in spontaneous resistant
301 mutants is not unexpected, since INH-resistance is caused by mutations in *inhA* in
302 only 2% of clinical isolates[26].

303

304 We demonstrate that THPPs potently suppress mycolic acid biosynthesis (**Fig. 3 and**
305 **Supplementary Fig. 1**). This phenotypic effect is distinct from other WGS-confirmed
306 MmpL3 inhibitors, such as SQ109[13] and BM212[8] (**Supplementary Fig. 2**). Previous
307 studies have used high concentrations of MmpL3 inhibitors (ranging from 3 × to 10 ×
308 MIC) and it is conceivable that the significant accumulation of TMM may be a result
309 of a stress response. However, the frequency of the MmpL3 resistance phenotype and
310 the increased sensitivity to THPPs upon overexpression of *mmpL3* gives credence to
311 the possibility of MmpL3 moonlighting as a drug importer.

312

313 Importantly, we demonstrate that *echA6* is essential in mycobacteria and is conserved
314 across several mycobacterial genomes (**Supplementary Table 6**), including the
315 'essential' minimal *M. leprae* genome[27]. Although the exact function of EchA6
316 remains to be established, we show that EchA6 has a distinct preference for long-

317 chain acyl-CoAs and interacts with selective components of FAS-II. We postulate that
318 EchA6 acts as a shuttle for fatty acid transfer, bypassing the non-essential FabH[28].
319 Overall, this would be compatible with its catalytically silent state, potential partners
320 identified by STRING analysis (**Supplementary Fig. 5**)[29] and its unique extended
321 acyl-CoA binding groove relative to the other 20 mycobacterial EchAs. The diversity
322 of crotonase family members in terms of enzymatic activity and substrates (albeit all
323 CoA-linked) leaves the door open to an alternative, as yet unidentified catalytic
324 activity. Emerging from these considerations is a model (**Fig. 3f**) that places EchA6 at
325 a critical junction between FAS-I, β-oxidation and FAS-II pathways.
326
327 In conclusion, we have shown that THPPs mediate bactericidal activity in a mouse
328 infection model of tuberculosis and that these compounds act on the catalytically
329 silent enoyl-CoA hydratase-like EchA6 protein. This surprising result of our
330 alternative target deconvolution approach suggests that spontaneous resistance-
331 conferring mutations can potentially obscure the actual target or alternative targets of
332 inhibitors emerging from phenotypic screening campaigns.
333
334

Supplementary information is linked to the online version of the paper.

Acknowledgements: GSB acknowledges support in the form of a Personal Research Chair from Mr. James Bardrick and a Royal Society Wolfson Research Merit Award. The research leading to these results has received funding from the European Union´s 7th framework programme (FP7- 2007-2013) under Grant Agreement No 261378 and the BBSRC through an Industrial CASE studentship. We thank Nico Zinn and Toby Mathieson for mass spectrometry and database design, Sarah Batt, Patrick Moynihan and Luke Alderwick for technical support. We also thank the TB Alliance for their helpful discussions and expertise in the field.

Author contributions: Conceived and designed the experiments: JAGC, KAA, SGD, UK, MB, GD, NCC, AB, LB, DB, KF, GSB. Performed the experiments: JAGC, KAA, IAB, SB, CA, AB, AS, PJJ, SGD, VN, SSG, MJR, LE, JR. Analyzed the data: KAA, JAGC, JR, SB, SGD, UK, MB, SGD, DB, LB, KF, GSB. Contributed reagents/materials/analysis tools: LB, MJP, GSB. Wrote the paper: JAGC, KAA, LB, DB, SGD, GD, CA, AB, KF, GSB.

Author information: Data deposition: The atomic coordinates and structure factors reported in this paper are deposited in the Protein Data Bank and shown in **Supplementary Table 5**.

Competing financial interests: The authors declare no competing financial interests.

357 **Figures Legends**

358

359 **Figure 1. THPP chemical structures and *in vivo* anti-tubercular activity.** (**a**)
360 Synthesis of THPPs. (**b**) *M. tuberculosis* H37Rv, *M. bovis* BCG, anti-bacterial and
361 cytotoxicity profile of THPPs. The human biological samples were sourced ethically
362 and their research use was in accordance with the terms of informed consent. (**c**)
363 Efficacy of GSK951A against an established murine model of *M. tuberculosis* chronic
364 infection. Mean ± SD is shown for each treated mice group (*n* = 3-7 mice/group). (**d**)
365 The ED_{99} of GSK951A and INH in a murine model of *M. tuberculosis* acute
366 infection[22] using *M. tuberculosis* transformed with either a multi-copy plasmid-borne
367 empty vector control, *echA6* or *echA6*^{W133A}. LogCFU counts are shown as the
368 difference with respect to the untreated control group infected with each strain
369 (ΔlogCFU/mouse). (**e**) The relative growth of each strain used in panel *d*. For both
370 panels (*d*,*e*), each data point represents an individual mouse. All animal studies were
371 ethically reviewed and carried out in accordance with European Directive 210/63/EU
372 and the GSK Policy on the Care, Welfare and Treatment of Animals.

373

374 **Figure 2: Chemoproteomics profiling identifies the putative enoyl-CoA**
375 **hydratase EchA6 as target of the THPP series.** (**a**) EchA6 is captured from *M.*
376 *bovis* BCG extracts with beads derivatized with GSK729. (**b**) EchA6 binds to beads
377 derivatized with the active enantiomer analogue GSK729 but not the inactive
378 enantiomer analogue GSK730. Binding is only competed by the active enantiomer
379 (**Supplementary Table 1** and **2**). (**c**) Estimation of the affinity of GSK729 for EchA6
380 (**Supplementary Table 3**).

381

382 **Figure 3. GSK951A inhibition of mycolic acid biosynthesis, resistance and**
383 **protein-protein interaction studies.** (**a,b**) [^{14}C]-Acetate labeling and dose-response
384 of GSK951A, INH and TLM against *M. bovis* BCG. Total MAMES and FAMES (*a*,
385 left and right panels, *n* = 3 biological replicates), reverse-phase TLC (*b*, *n* = 2
386 biological replicates) and cell wall bound MAMES (*a*, middle panel, *n* = 2 biological
387 replicates) were isolated and equal counts for the former two, and an equal aliquot for
388 the latter were analysed by TLC[13,14,30]. (**c**) SDS-PAGE (left panel) and Western blot
389 (right panel) analysis of pVV16 and pVV16-*echA6* cytosolic lysates (*n* = 3 biological
390 replicates). (**d**) Overexpression of *M. tuberculosis* EchA6 using pVV16-*echA6* in *M.*
391 *bovis* BCG (*n* = 5 biological replicates). (**e**) Protein-protein interaction screen using
392 the bacterial two-hybrid system BACTH and EchA6 with components of FAS-II (*n* =
393 3 biological replicates). (**f**) Proposed biosynthetic model linking FAS-I, FAS-II and
394 the β-oxidation pathways, providing a key role for EchA6 as a conduit for supplying
395 acyl-CoA primers for mycolic acid biosynthesis.
396
397 **Figure 4. Saturation binding assay using intrinsic tryptophan fluorescence to**
398 **quantify association of EchA6 with acyl-CoAs and THPPs.** (**a**) Saturation binding
399 curves for C_4-CoA, C_{12}-CoA, and C_{20}-CoA. (**b**) Comparison of saturation binding of
400 GSK951A between EchA6 and EchA6^{W133A}. (**c,d**) Competition binding assay of C_{20}-
401 CoA and C_4-CoA in the presence of 0–10 μM GSK951A. K_d values (mean ± SD)
402 resulting from non-linear least squares fitting of a single-site binding model are listed
403 in **Supplementary Table 4**. Data were fitted using GraphPad Prism.
404
405 **Figure 5. Structural features of EchA6 in the free and C_{20}-CoA bound state.** (**a**)
406 Ribbon diagram of the EchA6 monomer, bound to C_{20}-CoA (yellow sticks).

407 Secondary structure elements are labeled analogous to the structure of RnECH[23]. (**b**)
408 Ribbon diagram of the EchA6 trimer superimposed with the structure of *R.*
409 *norvegicus* enoyl-CoA hydratase (RnECH). EchA6 subunits are beige, green and
410 blue, RnECH is cyan. (**c**) Molecular surface of the 'front' and 'back' face of the
411 EchA6 trimer bound to C_{20}-CoA (subunit A in green). The binding sites of the
412 inhibitor GSK951A are indicated for subunits B and C by the stick model in cyan. (**d**)
413 Superposition of the active sites of RnECH (cyan) and EchA6 (yellow). Dashed lines
414 indicate the H-bond interactions that mediate polarization of the keto-moiety of CoA
415 in the hydratase reaction.
416
417 **Figure 6**. **Binding site of GSK951A in EchA6.** (**a**) The molecular surface of EchA6
418 is shown in translucent rendering and amino acid side chains within a 4 Å radius
419 around the ligand are shown as sticks. The σ_A-weighted 2Fo-Fc density map is
420 contoured at 1.0 σ and was calculated with coordinates of GSK951A included in the
421 model. (**b**) Superposition of GSK951A (carbon atoms in cyan) and CoA-bound
422 structure of EchA6. The thioester sulfur (green) of C_{20}-CoA is indicated. (**c**)
423 Schematic diagram of contacts between GSK951A and EchA6. Polar contacts are
424 indicated with a dashed line, vdW and hydrophobic contacts with a hashed line.
425

Figure 1

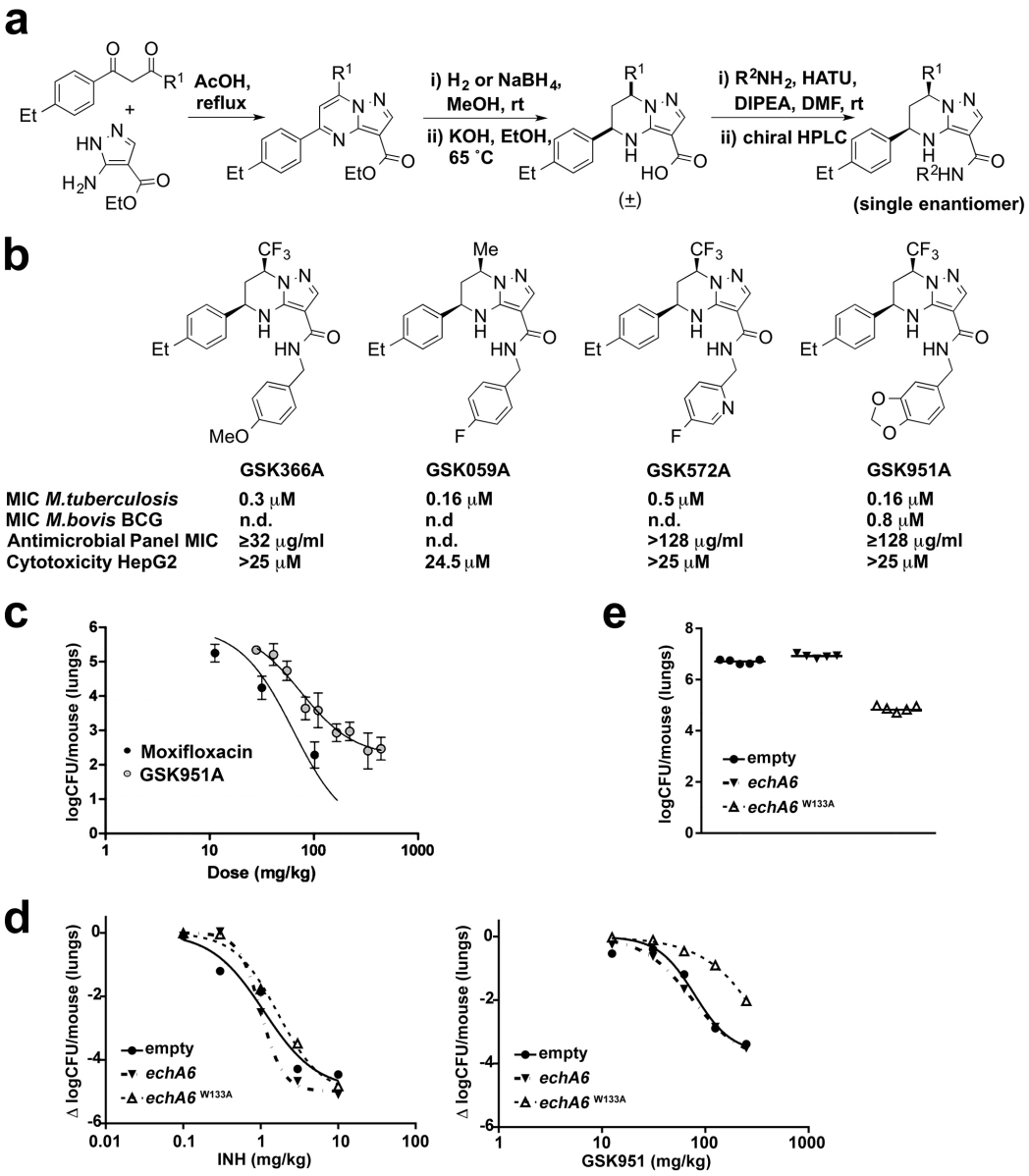
a
AcOH, reflux
i) H2 or NaBH4, MeOH, rt
ii) KOH, EtOH, 65 °C
i) R2NH2, HATU, DIPEA, DMF, rt
ii) chiral HPLC
(±)
(single enantiomer)
b
GSK366A
GSK059A
GSK572A
GSK951A
MIC M.tuberculosis 0.3 μM 0.16 μM 0.5 μM 0.16 μM
MIC M.bovis BCG n.d. n.d n.d. 0.8 μM
Antimicrobial Panel MIC ≥32 μg/ml n.d. >128 μg/ml ≥128 μg/ml
Cytotoxicity HepG2 >25 μM 24.5 μM >25 μM >25 μM
c
logCFU/mouse (lungs)
Moxifloxacin
GSK951A
Dose (mg/kg)
e
logCFU/mouse (lungs)
empty
echA6
echA6 W133A
d
Δ logCFU/mouse (lungs)
empty
echA6
echA6 W133A
INH (mg/kg)
GSK951 (mg/kg)

Figure 2

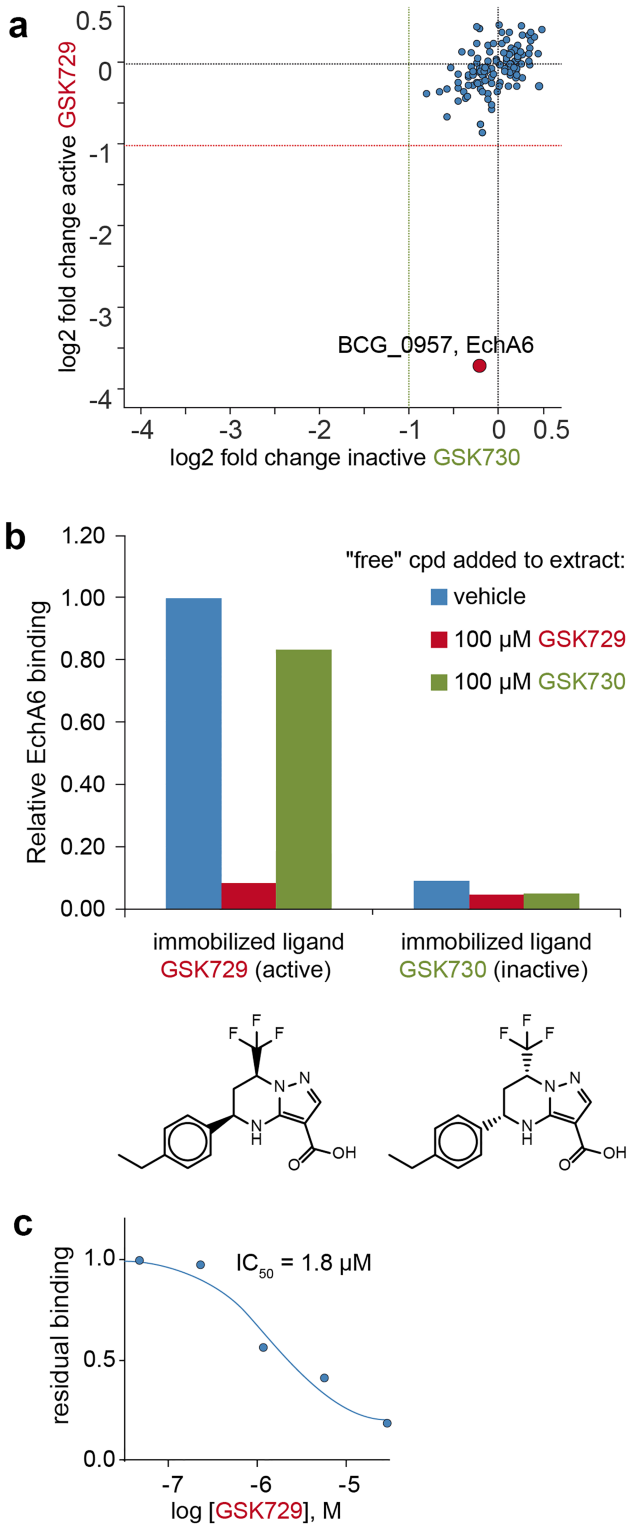
a
log2 fold change active GSK729
log2 fold change inactive GSK730
BCG_0957, EchA6
b
Relative EchA6 binding
"free" cpd added to extract:
vehicle
100 μM GSK729
100 μM GSK730
immobilized ligand GSK729 (active)
immobilized ligand GSK730 (inactive)
c
residual binding
IC50 = 1.8 μM
log [GSK729], M

Figure 3

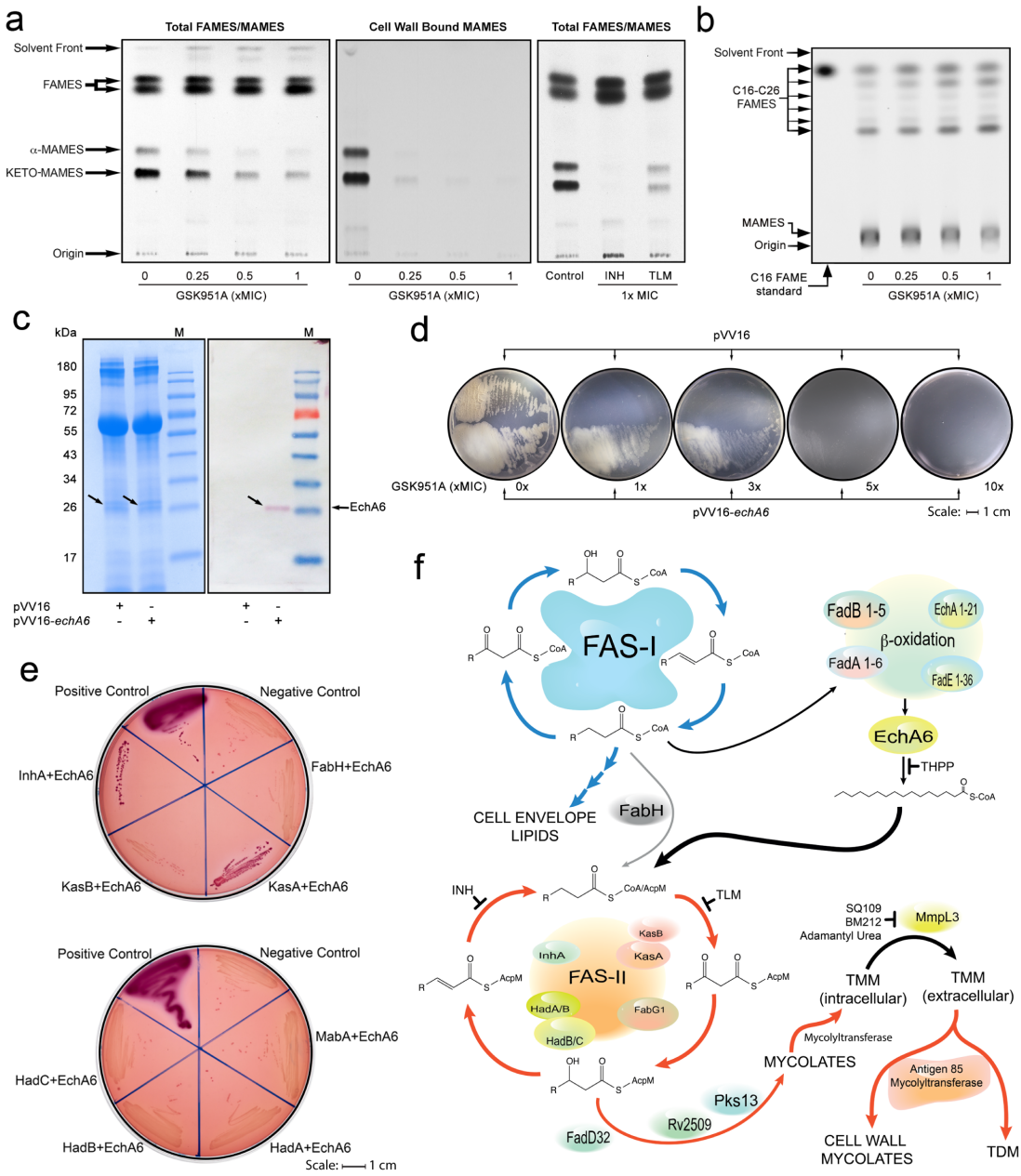
a
Total FAMES/MAMES
Cell Wall Bound MAMES
Total FAMES/MAMES
Solvent Front
FAMES
α-MAMES
KETO-MAMES
Origin
0
0.25
0.5
1
GSK951A (xMIC)
Control
INH
TLM
1x MIC
b
Solvent Front
C16-C26 FAMES
MAMES
Origin
C16 FAME standard
c
kDa
M
180
95
72
55
43
34
26
17
EchA6
pVV16
pVV16-echA6
d
pVV16
GSK951A (xMIC)
0x
1x
3x
5x
10x
pVV16-echA6
Scale: 1 cm
e
Positive Control
Negative Control
InhA+EchA6
FabH+EchA6
KasB+EchA6
KasA+EchA6
Positive Control
Negative Control
MabA+EchA6
HadC+EchA6
HadB+EchA6
HadA+EchA6
Scale: 1 cm
f
FAS-I
CoA
FadB 1-5
EchA 1-21
β-oxidation
FadA 1-6
FadE 1-36
EchA6
THPP
S-CoA
CELL ENVELOPE LIPIDS
FabH
INH
TLM
CoA/AcpM
AcpM
KasB
KasA
InhA
FAS-II
HadA/B
FabG1
HadB/C
FadD32
Rv2509
Pks13
MYCOLATES
SQ109
BM212
Adamantyl Urea
MmpL3
TMM (intracellular)
TMM (extracellular)
Mycolyltransferase
Antigen 85 Mycolyltransferase
CELL WALL MYCOLATES
TDM

445 **Figure 4**

446

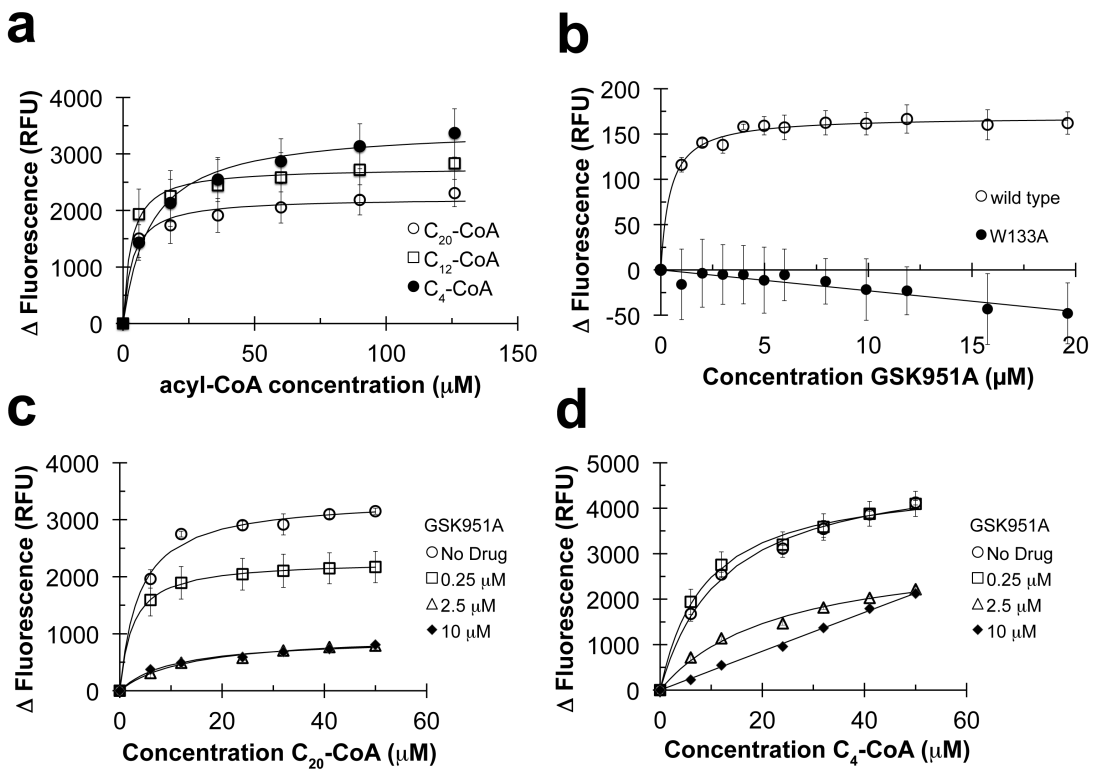

447
448
449
450
451
452
453
454
455
456
457
458
459
460
461
462
463
464
465

465 **Figure 5**
466
467
468
469

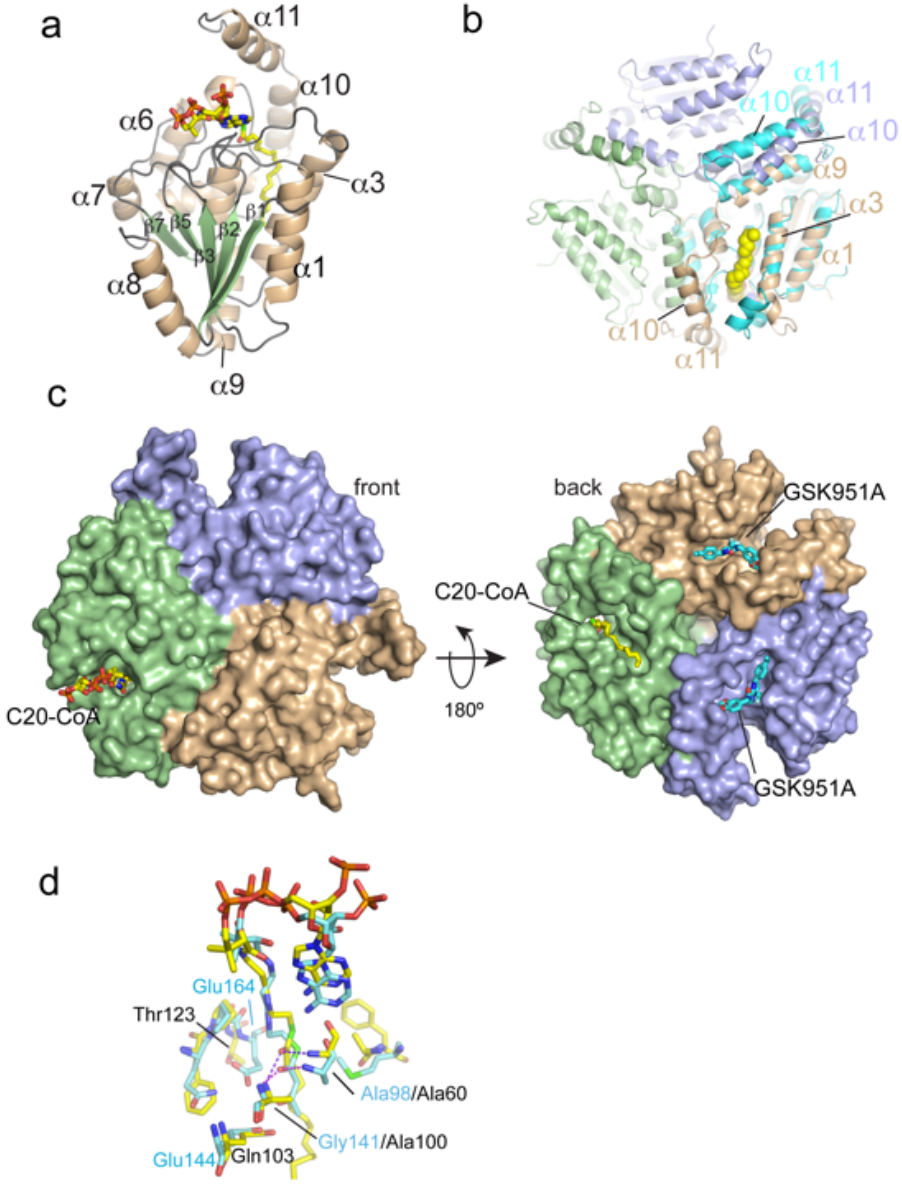

470
471
472
473
474

Figure 6

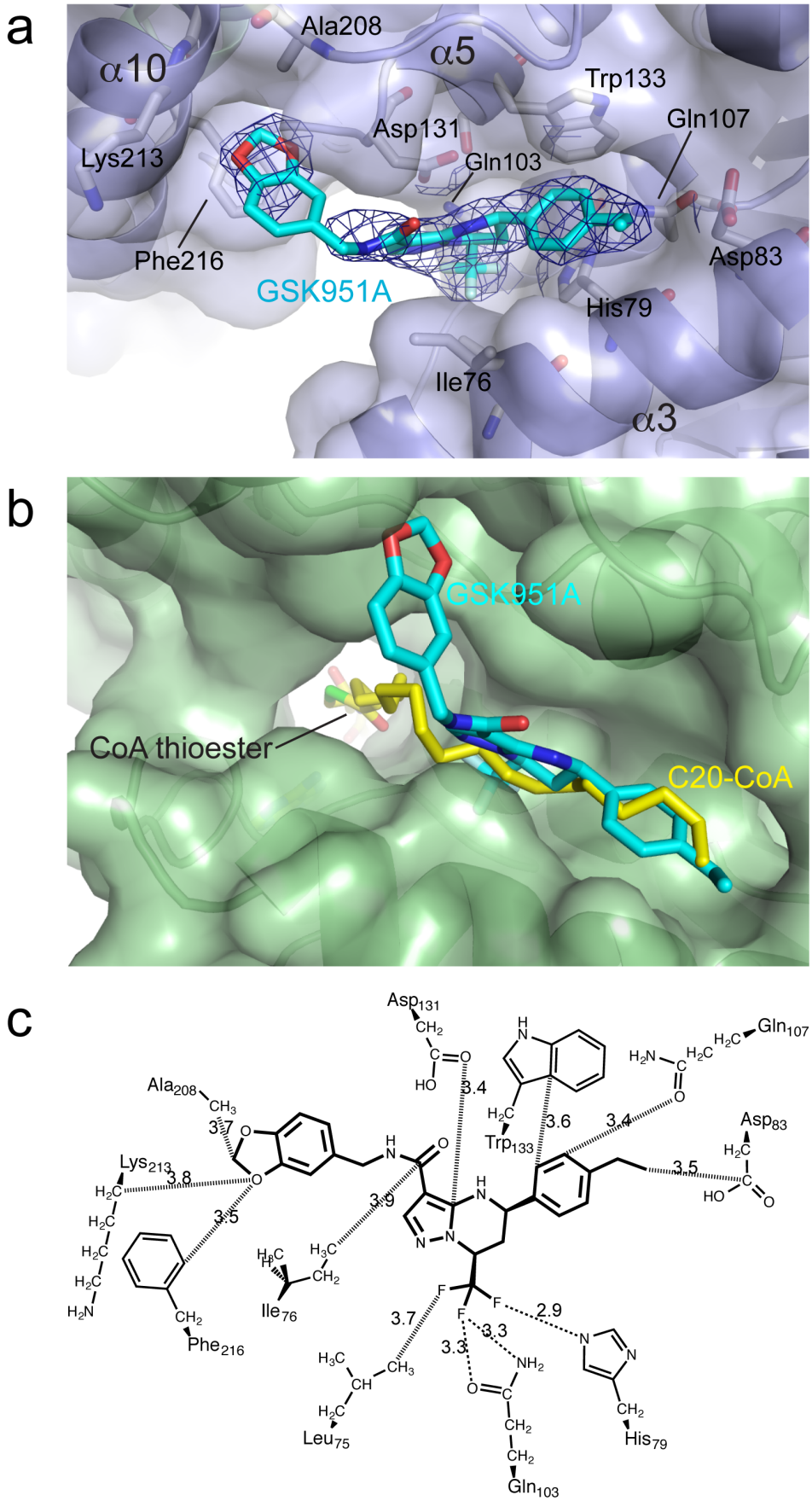
a
Ala208
α10
α5
Trp133
Gln107
Asp131
Lys213
Gln103
Phe216
Asp83
GSK951A
His79
Ile76
α3
b
GSK951A
CoA thioester
C20-CoA
c
Asp131
Gln107
Ala208
Asp83
Lys213
Trp133
Phe216
Ile76
Leu75
His79
Gln103
3.4
3.6
3.4
3.5
3.8
3.7
3.5
3.9
3.7
3.3
3.3
2.9

477 **Methods**

478

479 **General information for chemical synthesis**

480

481 Automated flash chromatography was performed on a Biotage FlashMaster II system
482 with peak detection at 254 nm. ^{1}H NMR spectra were recorded at 400 MHz on a
483 Bruker Ultrashield DPX 400 spectrometer. Chemical shifts (δ) are given in ppm
484 relative to the solvent reference as an internal standard (DMSO-d_6, δ = 2.50 ppm;
485 $CDCl_3$, δ = 7.27 ppm). Data are reported as follows: chemical shift (multiplicity (s for
486 singlet, d for doublet, t for triplet, q for quartet, m for multiplet, br for broad),
487 integration, coupling constant(s) in Hz). HPLC–MS analyses were conducted on an
488 Agilent 1100 instrument equipped with a Sunfire C18 column (30 × 2.1 mm i.d., 3.5
489 mm packing diameter) at 40ºC coupled with a Waters ZMD2000 mass spectrometer;
490 the method of ionization was alternate-scan positive and negative electrospray. Semi-
491 preparative chiral HPLC was conducted on an Agilent 1100 instrument equipped with
492 a Chiralpak IC column (250 mm x 20 mm). Preparative chiral HPLC was conducted
493 on a Varian SD-2 prep HPLC instrument equipped with a Chiralpak IC column (250
494 mm x 50 mm i.d, 20 µm packing diameter). Compounds had a purity of >95 %, as
495 determined by HPLC and ^{1}H NMR analysis.

496

497 **Ethyl 7-(4-ethylphenyl)-7-methylpyrazolo[1,5-a]pyrimidine-3-carboxylate.** A
498 mixture of ethyl 3-aminopyrazole-4-carboxylate (2.99 g, 19.24 mmol), 1-(4-
499 ethylphenyl)-1,3-butanedione (3.66 g, 19.24 mmol) and acetic acid (15 ml) was
500 heated at reflux for 6 h. LC-MS analysis showed an 80/20 mixture of two products.
501 After cooling to room temperature, the reaction mixture was poured onto ice (60 g).

502 The solid formed was filtered off, triturated with hexane and dried to afford a pale
503 yellow solid. The crude product was added to a silica gel column (40 g) and eluted
504 with a mixture of EtOAc/hexane (gradient 0-20 %). Collection of the appropriate
505 fractions afforded the desired compound (747 mg, 2.42 mmol, 13 %) as a white solid
506 along with a regioisomeric by-product (2.98 g, 9.63 mmol, 50 %). ^{1}H NMR (400
507 MHz, $CDCl_3$+D_2O) δ ppm: 8.58 (s, 1H), 8.15-8.17 (m, 2H), 7.35-7.37 (m, 2H), 7.33
508 (s, 1H), 4.46 (q, 2H, *J*=7.1), 2.89 (s, 1H), 2.74 (q, 2H, *J*=7.6), 1.48 (t, 3H, *J*=7.1), 1.30
509 (t, 3H, *J*=7.6).
510
511 ***cis*-Ethyl 5-(4-ethylphenyl)-7-methyl-4,5,6,7-tetrahydropyrazolo[1,5-**
512 **a]pyrimidine-3-carboxylate.** To a solution of ethyl 5-(4-ethylphenyl)-7-
513 methylpyrazolo[1,5-a]pyrimidine-3-carboxylate (710 mg, 2.30 mmol) in anhydrous
514 methanol (10 ml), 10 % Pd/C (244 mg, 0.23 mmol) was added. The reaction was
515 hydrogenated at 40 psi for 24 h. LC-MS showed completion of the reaction. The
516 mixture was filtered over celite and concentrated *in vacuo* affording the desired
517 compound (714 mg, 2.23 mmol, 99 %) as a white solid. The product was used in the
518 next step without further purification. ^{1}H NMR (400 MHz, $CDCl_3$+D_2O) δ ppm: 7.66
519 (s, 1H), 7.33-7.35 (m, 2H), 7.22-7.24 (m, 2H), 5.93 (bs, 1H), 4.56 (dd, 1H, *J*=11.6 and
520 2.8), 4.28-4.36 (m, 1H), 4.24 (q, 2H, *J*=7.1), 2.68 (q, 2H, *J*=7.6), 2.29-2.35 (m, 1H),
521 2.00 (dt, 1H, *J*=13.4 and 11.1), 1.61 (d, 3H, *J*=6.3), 1.32 (t, 3H, *J*=7.1), 1.26 (t, 3H,
522 *J*=7.6).
523
524 ***cis*-5-(4-Ethylphenyl)-7-methyl-4,5,6,7-tetrahydropyrazolo[1,5-a]pyrimidine-3-**
525 **carboxylic acid.** To a solution of *cis*-ethyl 5-(4-ethylphenyl)-7-methyl-4,5,6,7-
526 tetrahydropyrazolo[1,5-a]pyrimidine-3-carboxylate (700 mg, 2.23 mmol) in ethanol
527 (5 ml), a 1.5 M KOH aqueous solution (5.21 ml, 7.82 mmol) was added and the

528 reaction was stirred at 60ºC for 12 h. The reaction was concentrated *in vacuo* to
529 remove the organic solvent and a saturated citric acid solution was then added until
530 acidic pH. The solid was collected by filtration, washed with water and dried to afford
531 the desired compound (539 mg, 1.89 mmol, 85 %) as a white solid. ^{1}H NMR (400
532 MHz, DMSO-d_6) δ ppm: 11.8 (bs, 1H), 7.49 (s, 1H), 7.33-7.35 (m, 2H), 7.22-7.24 (m,
533 2H), 6.04 (bs, 1H), 4.58 (dd, 1H, *J*=11.1 and 2.3), 4.22-4.32 (m, 1H), 2.61 (q, 2H,
534 *J*=7.6), 2.25-2.35 (m, 1H), 1.87 (dt, 1H, *J*=13.1 and 10.9), 1.43 (d, 3H, *J*=6.3), 1.18 (t,
535 3H, *J*=7.6). [ES+ MS] m/z 286 (M+H)+.
536
537 **(*5R*,7*R*)-*N*-(4-fluorobenzyl)-5-(4-ethylphenyl)-7-methyl-4,5,6,7-**
538 **tetrahydropyrazolo-[1,5-a]pyrimidine-3-carboxamide (GSK059A).** To a solution
539 of *cis*-5-(4-ethylphenyl)-7-methyl-4,5,6,7-tetrahydropyrazolo[1,5-a]pyrimidine-3-
540 carboxylic acid (100 mg, 0.35 mmol) in *N*,*N*-dimethylformamide (3 ml), HATU (160
541 mg, 0.42 mmol) and *N*,*N*-Disopropylethylamine (0.306 ml, 1.75 mmol) were added.
542 The mixture was stirred at room temperature for 30 min. (4-
543 fluorophenyl)methanamine hydrochloride (85 mg, 0.53 mmol) was added and the
544 mixture was stirred at 60ºC for 3 days. LC-MS showed the desired product as major
545 and no starting material. After cooling to room temperature, the reaction mixture was
546 diluted with TBME and washed with saturated NH_4Cl aqueous solution and brine.
547 The organic layers were concentrated and the residue was added to a silica gel column
548 (5 g) and eluted with a mixture of EtOAc/cyclohexane (gradient 0-60 %). Collection
549 of the appropriate fractions afforded the desired racemic compound (116 mg, 0.296
550 mmol, 84 %) as a white solid. The enantiomers were separated by semipreparative
551 HPLC (flow: 18 ml/min; solvent: hexane/EtOH 90/10; column: Chiralpak IC, 250
552 mm x 20 mm). The desired enantiomer eluted at 15 min and the opposite at 23 min.

553 The title compound was obtained (35 mg, 0.089 mmol) as a white solid
554 enantiomerically pure by HPLC. ^{1}H NMR (400 MHz, $CDCl_3$) δ ppm: 7.50 (bs, 1H),
555 7.27-7.34 (m, 4H), 7.20-7.22 (m, 2H), 6.99-7.04 (m, 2H), 6.47 (bs, 1H), 5.94 (bs, 1H),
556 4.44-4.58 (m, 3H), 4.27-4.37 (m, 1H), 2.66 (q, 2H, *J*=7.6), 2.28-2.36 (m, 1H), 1.96-
557 2.08 (m, 2H), 1.61 (d, 3H, *J*=6.1), 1.25 (t, 3H, *J*=7.8). [ES+ MS] m/z 393 (M+H)+.
558
559 **(5-Fluoropyridin-2-yl)methanamine dihydrochloride.** A mixture of 5-
560 fluoropicolinonitrile (300 mg, 2.457 mmol), 10 % wt. palladium on carbon (60 mg,
561 0.056 mmol), methanol (25 ml) and concentrated HCl (1 ml, 11.70 mmol) was stirred
562 at room temperature under 30 psi of hydrogen. After 4 h the reaction was filtered
563 through celite washing with 200 ml of methanol. Evaporation afforded the desired
564 compound (500 mg, 2.39 mmol, 97%) as an off-white solid. ^{1}H NMR (400 MHz,
565 DMSO-d_6) δ ppm: 8.32-9.32 (m, 4H), 8.63 (d, 1H, *J*=2.8), 7.84 (td, 1H, *J*=8.8 and
566 3.0), 7.64 (dd, 1H, *J*=8.6 and 4.3), 4.17 (bq, 2H, *J*=5.8).
567
568 **(5R,7S)-5-(4-ethylphenyl)-N-((5-fluoropyridin-2-yl)methyl)-7-(trifluoromethyl)-**
569 **4,5,6,7-tetrahydropyrazolo[1,5-a]pyrimidine-3-carboxamide (GSK572A).** To a
570 solution of *cis*-5-(4-ethylphenyl)-7-(trifluoromethyl)-4,5,6,7-tetrahydropyrazolo[1,5-
571 a]pyrimidine-3-carboxylic acid (200 mg, 0.589 mmol) in *N*,*N*-dimethylformamide (5
572 ml) at room temperature under nitrogen, HATU (269 mg, 0.707 mmol) was added
573 followed by *N*,*N*-diisopropylethylamine (0.309 ml, 1.768 mmol). The mixture was
574 stirred at room temperature for 15 min and then a solution of (5-fluoropyridin-2-
575 yl)methanamine dihydrochloride (153 mg, 0.766 mmol) and *N*,*N*-
576 diisopropylethylamine (0.309 ml, 1.768 mmol) in *N*,*N*-dimethylformamide (3 ml) was
577 added. The mixture was stirred at room temperature for 3 days. The reaction mixture

578 was diluted with EtOAc (30 ml) and washed with saturated aqueous $NaHCO_3$ (3 x 40
579 ml), water (40 ml) and 1M NH_4Cl (3 x 40 ml). The organic layer was dried, filtered
580 and evaporated. The residue was added to a silica gel column and eluted with a
581 mixture of EtOAc/cyclohexane (gradient 0-100 %). Collection of the appropriate
582 fractions afforded the desired racemic compound (221 mg, 0.469 mmol, 80 %) as an
583 off-white solid. The enantiomers were separated by semipreparative HPLC (flow: 18
584 ml/min; solvent: hexane/EtOH 90/10; column: Chiralpak IC, 250 mm x 20 mm). The
585 desired enantiomer (GSK572A) eluted at 15 min and the opposite (GSK573A) at 23
586 min. The title compound was obtained (93 mg, 0.197 mmol) as a white solid
587 enantiomerically pure by HPLC. ^{1}H NMR (400 MHz, $CDCl_3$) δ ppm: 8.42 (d, 1H,
588 *J*=2.8), 7.63 (s, 1H), 7.31-7.42 (m, 4H), 7.22-7.24 (m, 2H), 6.60-6.64 (m, 2H), 4.81-
589 4.89 (m, 1H), 4.66 (dd, 1H, *J*=16.7 and 5.3), 4.62 (dd, 1H, *J*=16.7 and 5.3), 4.54 (dd,
590 1H, *J*=11.6 and 2.5), 2.67 (q, 2H, *J*=7.6), 2.50-2.56 (m, 1H), 2.33-2.42 (m, 1H), 1.25
591 (t, 3H, *J*=7.8). [ES+ MS] m/z 448 (M+H)+.
592
593 **General methods**
594
595 The measurement of the MIC for each tested compound, general antimicrobial
596 activity, microsomal fraction stability, pharmacokinteic studies, HepG2 cytotoxicity
597 assay, SDS-PAGE and Western blot were performed as described previously[2,19,30].
598 *EchA6* (*Rv0905*) was cloned into the mycobacterial multi-copy plasmid pMV261 and
599 its derivatives[30]; the site-directed mutant EchA6^{W133A} was generated using the
600 plasmids containing wild-type *echA6* and QuikChange II (Agilent Technologies).
601 *MmpL3* (*Rv0206c*) was cloned into pMV261. The constructs were electroporated into
602 either *M. bovis* BCG or *M. tuberculosis*. The primers are described in **Supplementary**

603 **Table 7**. The *in vitro* effect of GSK951A, TLM, and INH was studied by treating *M.*
604 *bovis* BCG cultures at OD_{600} of 0.4 with inhibitor for 24 hours, followed by [^{14}C]-
605 acetate labeling for 24 hours, and subsequent analysis of either total FAMES and
606 MAMES (equal counts, typically 30,000 cpm), cell wall bound MAMES (equal
607 volumes, 5 % aliquot), or cell envelope lipids (equal counts, typically 30,000 cpm) as
608 described previously[13,14,19,30-32]. Protein-protein interactions were studied using the
609 bacterial adenylate cyclase based two-hybrid system as described[33]. Briefly, *echA6*
610 (*Rv0905*) was cloned using the primers described in **Supplementary Table 7** into
611 pUT18 in-frame with the T18 fragment, and the FAS-II genes cloned into pKT25 in-
612 frame with the T25 fragment. The positive control pKT25 was fused to the Leucine
613 Zipper of GCN4 co-transformed with pUT18C of the Leucine Zipper GCN4. The
614 negative control was pKT25 Zip co-transformed with empty pUT18 vector. The GSK
615 in-house hydrophobicity assay was performed using 10 μl of a 10 mM DMSO stock
616 solution diluted to 750 μl with octanol saturated phosphate buffer pH 7.4 and 160 μl
617 buffer saturated octanol in a 96-well deep well block. Blocks were sealed and inverted
618 for 3 sets of 50 inversions, then centrifuged at 300 *g* for 20 min. Both phases were
619 quantified using generic gradient UV-HPLC.
620
621 **Assessment of chronic and acute efficacy in murine TB models**
622
623 The assessment of the chronic and acute efficacy in murine TB models was performed
624 using specific pathogen-free, 8-10 week-old female C57BL/6 mice purchased from
625 Harlan Laboratories and allowed to acclimate for one week. In the chronic model,
626 mice (*n* = 3-7 mice per dose level, a total of 27/28 mice per compound) were
627 intratracheally infected with 100 CFU/mouse and GSK951A formulated in 1 %

628 aqueous methylcellulose and administered daily for 8 consecutive weeks, starting 6
629 weeks after infection. Lungs were harvested 24 h after the last administration. All
630 lung lobes were aseptically removed, homogenized and frozen. Homogenates were
631 plated on 10 % OADC-7H11 medium supplemented with activated charcoal (0.4 %)
632 for 18 days at 37ºC. In the acute model[22], mice were intratracheally infected with
633 50,000 CFU/mouse with all strains, and lungs harvested on day 9. GSK951A and INH
634 (in water) were administered daily for 8 consecutive days, starting on day 1 after
635 infection. All lung lobes were aseptically removed, homogenized, and plated in 10 %
636 OADC-7H11 medium supplemented with activated charcoal (0.4 %) and grown for
637 18-25 days at 37ºC. Lung logCFUs *vs* dose was fitted to a logistic equation (sigmoidal
638 dose response, variable slope, GraphPad Prism software). Effective dose 99 % (ED_{99}),
639 defined as the dose in mg/kg that reduced lung bacterial burden at day 9 after
640 infection by 99 % (2 logCFU) with respect to untreated, was calculated by
641 interpolation in the sigmoidal curve. The number of mice was selected as the
642 minimum number of mice that is necessary to detect a 3-fold difference in the ED_{99} of
643 two different products. Mice were randomly allocated to the different experimental
644 groups immediately after the infection.
645
646 **Preparation of *M. bovis* BCG cytosolic extract**
647
648 *M. bovis* BCG cell pellets were resuspended in lysis buffer (50 mM Tris-HCl, pH 7.4,
649 1 mM EDTA, 7.5 % glycerol, 150 mM NaCl, 25 mM NaF, 1 mM Na_3VO_4, 1 mM
650 DTT, and 1 complete EDTA-free protease inhibitor tablet (Roche) *per* 25 ml). After
651 sonication the samples were adjusted to 0.8 % Igepal-CA630 and extraction was
652 completed by homogenization using a Dounce homogenizer. After 45 min rotation at

653 4ºC, the samples were subjected to centrifugation for 10 min at 20,000 *g* at 4ºC. The
654 supernatant was kept on ice, while the pellet was re-extracted with 1 volume of lysis
655 buffer adjusted to 0.8 % Igepal-CA630. The pellet was resuspended using a long 20
656 gauge needle (2x), followed by rotation for 30 min at 4ºC. After a centrifugation step
657 as described above, both supernatants were pooled and subjected to centrifugation at
658 100,000 *g* for 1 h at 4ºC. The final supernatant was snap frozen in liquid nitrogen and
659 stored at -80ºC.
660
661 **Chemoproteomics**
662
663 Sepharose beads were derivatized with GSK729A at various concentrations from 0.05
664 mM to 2 mM. Beads (35 µl) were washed and equilibrated in lysis buffer incubated at
665 4ºC for 1 h with 1 ml (1 mg) *M. bovis* BCG cytosolic extract, which was pre-
666 incubated with compound or buffer. Beads were transferred to disposable columns
667 (MoBiTec), washed extensively with lysis buffer and eluted with SDS sample buffer.
668 Proteins were alkylated, separated on 4-12 % NuPAGE (Invitrogen), stained with
669 colloidal Coomassie, and quantified by isobaric tagging and LC-MS/MS. Digestion,
670 labeling with TMT isobaric mass tags, peptide fractionation, and mass spectrometric
671 analyses were performed essentially as described[16]. The proteins.fasta file for *M.*
672 *bovis* BCG was downloaded (May 11th 2011) from
673 http://genome.tbdb.org/annotation/genome/tbdb/MultiDownloads.html and
674 supplemented with the sequences of bovine serum albumin, porcine trypsin and
675 mouse, rat, sheep and dog keratins. Decoy versions of all proteins were created and
676 added. The search database contained a total of 11,492 protein sequences, 50 %
677 forward, 50 % reverse. Criteria for protein quantification were: a minimum of 2

678 sequence assignments matching to unique peptides (FDR for quantified proteins
679 <<0.1 %), Mascot ion score > 15, signal to background ratio of the precursor ion > 4,
680 signal to interference > 0.5[34]. Reporter ion intensities were multiplied with the ion
681 accumulation time yielding an area value proportional to the number of reporter ions
682 present in the mass analyzer. Peptide fold changes were corrected for isotope purity as
683 described and adjusted for interference caused by co-eluting nearly isobaric peaks as
684 estimated by the signal-to-interference measure[35]. Protein quantification was achieved
685 using a sum-based bootstrap algorithm[36].

686

687 **Generation and characterisation of a conditional *echA6* mutant in *M. bovis* BCG**

688

689 A conditional mutant in the *M. bovis* BCG homologue of *M. tuberculosis echA6* was
690 generated using the genetic tool CESTET[17,18]. First, a recombinant *echA6* knockout
691 phage was designed to replace the *M. bovis* BCG *echA6* homologue. The primers used
692 for amplifying the left and right flanks to generate the allelic exchange substrate[17,18]
693 are provided in **Supplementary Table 7**. Next, *Rv0905* was PCR amplified using the
694 primers mdRv0905_F and mdRv0905_R (**Supplementary Table 7**) and cloned
695 downstream of the tetracycline promoter into the integrating vector pTIC6a to
696 generate the plasmid pTIC6a-*Rv0905*[17,18]. A merodiploid strain was then constructed
697 by electroporating pTIC6a-*Rv0905* into *M. bovis* BCG. The resultant strain
698 BCG::*Rv0905* was then transduced with *echA6* knockout phage. Transductants were
699 selected on 7H10-agar plates containing 25 μg/ml kanamycin, 75 μg/ml hygromycin
700 and 50 ng/ml anhydrotetracycline (ATc). One confirmed knockout strain was called
701 Δ*BCG0957* and was used in a conditional depletion experiment to detect cell death as
702 shown previously in minimal medium[17,18].

703

704 **Recombinant production and purification of EchA6 and EchA6^{W133A}**

705

706 The gene *echA6* (*Rv0905*) was amplified by PCR (**Supplementary Table 7**) and
707 cloned into plasmid pET28a (Novagen). Briefly, *E. coli* BL21 (DE3) transformed
708 with pET28a-*echA6* or pET28a-*echA6*^{W133A} (through site-directed mutagenesis of
709 pET28a-*echA6*; the primers are described in **Supplementary Table 7**) were grown in
710 Luria Bertani (LB) broth from a glycerol stock (37ºC, 180 rpm, shaking), grown
711 overnight and used to inoculate flasks containing 1 L of LB media containing 50
712 μg/ml kanamycin. Bulk cultures were grown (37ºC, 180 rpm) shaking to OD_{600} = 0.4-
713 0.6, and induced with 1 mM IPTG, reducing the incubation temperature to 16ºC.
714 Batch culture was continued at 16ºC until 24 h post-induction at which point cultures
715 were harvested by centrifugation at 5,000 rpm at 4ºC and the pellets stored at –20ºC.
716 Cell pellets were defrosted and resuspended in 20 ml of lysis buffer (50 mM sodium
717 phosphate, 600 mM sodium chloride and 10 mM imidazole, pH 8) with a complete
718 EDTA-free Protease Inhibitor Cocktail Tablet (Roche), and sonicated on ice with 10
719 cycles of 30 sec sonication and 30 sec cooling, and centrifuged (40 min, 15,000 rpm,
720 4ºC). For purification of the His_6-tagged EchA6 (and EchA6^{W133A}) protein, a His-trap
721 HP column (GE Healthcare Life Sciences) was used following the manufacturers
722 guidelines using a step-wise gradient of 50 mM, 125 mM, 150 mM and 200 mM
723 imidazole in buffer. Eluates were analyzed by 12 % SDS-PAGE (Bio-Rad) run at 200
724 V, 50 mA for 40 min. Gels were stained with Instant Blue (Expedeon). Fractions
725 containing pure protein were dialyzed overnight in 2 L of dialysis buffer (25 mM
726 HEPES, 10 % glycerol and 300 mM NaCl, pH 8). EchA6 was then concentrated by

727 centrifugation to >30 mg/ml using a spin column (Thermo Scientific) and the
728 concentration of protein was determined by absorption spectroscopy at 280 nm.
729
730 **X-ray crystallographic structure determination**
731
732 Crystals of EchA6 in the ligand-free form and bound to THPP compounds or C_{20}-
733 CoA were obtained by vapour diffusion at 18ºC, using commercial sparse matrix
734 screens JCSG-*plus* and MIDAS (Molecular Dimensions) in 96-well sitting drop plates
735 (SWISSCI 3-lens). A liquid handling robot (Mosquito) was used to dispense 300 nl
736 drops consisting of 150 nl protein at concentrations between 20 and 30 mg/ml plus
737 150 nl reservoir solution. Complexes with ligands (C_{20}-CoA, THPPs) were grown in
738 the presence of 3-fold molar excess of ligand over protein. Reservoir conditions
739 leading to diffraction-quality crystals are: 0.1 M Tris pH 8.0 with 60 % v/v
740 polypropylene glycol 400 (*apo* EchA6); 0.17 M ammonium sulfate, 25.5 % w/v PEG
741 4K, 15 % v/v glycerol (EchA6:C_{20}-CoA); 0.1 M Tris pH 8.5 with 20 % v/v ethanol
742 (EchA6:366A); 0.6 M tri-sodium citrate cryoprotected with a 10 % glycerol additive
743 (EchA6:059A); 0.2 M sodium chloride, 0.1 M sodium cacodylate pH 6.5, 2 M
744 ammonium sulfate, cryoprotected with a 10 % ethylene glycol additive
745 (EchA6:572A); 0.1 M sodium cacodylate pH 6.5, 1.0 M tri-sodium citrate
746 cryoprotected with a 20 % glycerol additive (EchA6:951A). X-ray diffraction data
747 were recorded at the Diamond Light Source and on our in-house X-ray source
748 (Rigaku MicroMax 007HF, VariMax optics, Saturn 944 CCD detector). Details of the
749 X-ray data statistics are given in **Supplementary Table 5**. Data were reduced using
750 XDS, XSCALE[37] and analysed using the CCP4 suite of crystallographic software[38].
751 Using *M. tuberculosis* EchA6 (PDB entry 3HE2) as a search model, we determined

752 initial phases by molecular replacement (PHASER[39]). The models were rebuilt and
753 refined (COOT[40], REFMAC5[41], PHENIX.REFINE[42]), using non-crystallographic
754 symmetry restraints where the asymmetric unit contained 3 or 6 EchA6 subunits. Due
755 to the limited resolution of the corresponding X-ray data, grouped B-factors were
756 modelled when refining the complexes of EchA6:C_{20}-CoA, EchA6:GSK059A and
757 EchA6:GSK951A. Ligand geometry restraints were generated using the SKETCHER
758 utility of CCP4[38]. Figures of the molecular structures of EchA6 were prepared using
759 PyMOL (www.pymol.org). Refinement statistics are reported in **Supplementary**
760 **Table 5**. The Fo-Fc density maps (**Supplementary Fig. 4**) indicating the presence
761 and structures of the ligands were generated using phases of the protein model after
762 initial refinement of the molecular replacement solution and prior to incorporation of
763 the ligand in the coordinate model.
764
765 **Intrinsic tryptophan fluorescence ligand binding assays**
766
767 Fluorescence binding assays of EchA6 (3.75 μM) with acyl-CoAs were conducted on
768 a Hitachi F7000 Fluorescence Spectrophotometer using 25 mM HEPES, 10 %
769 glycerol and 300 mM NaCl, pH 8 at 25ºC and fluorescence spectra measured at an
770 excitation wavelength 280 nm and emission wavelength 300-400 nm with an
771 excitation and emission slit width of 5 nm using a 500 μl crystal cuvette. Ligands
772 were added at increasing stoichiometric ratios ranging from 0.5 to 8 times the molar
773 concentration of protein. DMSO concentrations were maintained at <0.6 % and <2.0
774 % in the assay mixture for acyl-CoA and THPP, respectively. Data were recorded
775 using Hitachi FL Solutions 4.6 software and analysed in Prism 5 (GraphPad). To
776 compare ligand binding between wild-type EchA6 and EchA6^{W133A}, the proteins were

777 dialysed against buffer 25 mM HEPES, 10 % glycerol and 300 mM NaCl, pH 8, 2 %
778 DMSO (v/v). Changes of fluorescence intensities were corrected for volume
779 expansion and for non-specific binding of DMSO.
780

780 **References**

781

782 1 WHO. *Global Tuberculosis Report 2013* (World Health Organization,
783 Geneva, 2013).

784 2 Abrahams, K. A. *et al.* Identification of novel imidazo[1,2-a]pyridine
785 inhibitors targeting *M. tuberculosis* QcrB. *PloS One* **7**, e52951 (2012).

786 3 Gurcha, S. S. *et al.* Biochemical and structural characterization of
787 mycobacterial aspartyl-tRNA synthetase AspS, a promising TB drug target.
788 *PloS One* **9**, e113568 (2014).

789 4 Mugumbate, G. *et al.* Mycobacterial dihydrofolate reductase inhibitors
790 identified using chemogenomic methods and in vitro validation. *PloS One* **10**,
791 e0121492 (2015).

792 5 Wang, F. *et al.* Identification of a small molecule with activity against drug-
793 resistant and persistent tuberculosis. *Proc. Natl. Acad. Sci. USA* **110**, E2510-
794 2517 (2013).

795 6 Andries, K. *et al.* A diarylquinoline drug active on the ATP synthase of
796 *Mycobacterium tuberculosis*. *Science* **307**, 223-227 (2005).

797 7 Grzegorzewicz, A. E. *et al.* Inhibition of mycolic acid transport across the
798 *Mycobacterium tuberculosis* plasma membrane. *Nat. Chem. Biol.* **8**, 334-341
799 (2012).

800 8 La Rosa, V. *et al.* MmpL3 is the cellular target of the antitubercular pyrrole
801 derivative BM212. *Antimicrob. Agents Chemother.* **56**, 324-331 (2012).

802 9 Li, K. *et al.* Multitarget drug discovery for tuberculosis and other infectious
803 diseases. *J. Med. Chem.* **57**, 3126-3139 (2014).

804 10 Li, W. *et al.* Novel insights into the mechanism of inhibition of MmpL3, a
805 target of multiple pharmacophores in *Mycobacterium tuberculosis*.
806 *Antimicrob. Agents Chemother.* **58**, 6413-6423 (2014).
807 11 Rao, S. P. *et al.* Indolcarboxamide is a preclinical candidate for treating
808 multidrug-resistant tuberculosis. *Sci. Transl. Med.* **5**, 214ra168 (2013).
809 12 Remuinan, M. J. *et al.* Tetrahydropyrazolo[1,5-a]pyrimidine-3-carboxamide
810 and N-benzyl-6',7'-dihydrospiro[piperidine-4,4'-thieno[3,2-c]pyran] analogues
811 with bactericidal efficacy against *Mycobacterium tuberculosis* targeting
812 MmpL3. *PloS One* **8**, e60933 (2013).
813 13 Tahlan, K. *et al.* SQ109 targets MmpL3, a membrane transporter of trehalose
814 monomycolate involved in mycolic acid donation to the cell wall core of
815 *Mycobacterium tuberculosis*. *Antimicrob. Agents Chemother.* **56**, 1797-1809
816 (2012).
817 14 Banerjee, A. *et al. inhA*, a gene encoding a target for isoniazid and
818 ethionamide in *Mycobacterium tuberculosis*. *Science* **263**, 227-230 (1994).
819 15 Zhang, Y., Heym, B., Allen, B., Young, D. & Cole, S. The catalase-peroxidase
820 gene and isoniazid resistance of *Mycobacterium tuberculosis*. *Nature* **358**,
821 591-593 (1992).
822 16 Bantscheff, M. *et al.* Chemoproteomics profiling of HDAC inhibitors reveals
823 selective targeting of HDAC complexes. *Nat. Biotechnol.* **29**, 255-265 (2011).
824 17 Brown, A. K. *et al.* Identification of the dehydratase component of the
825 mycobacterial mycolic acid-synthesizing fatty acid synthase-II complex.
826 *Microbiology* **153**, 4166-4173 (2007).

827 18 Rana, A. K. *et al.* Ppm1-encoded polyprenyl monophosphomannose synthase
828 activity is essential for lipoglycan synthesis and survival in mycobacteria.
829 *PloS One* **7**, e48211 (2012).
830 19 Kremer, L. *et al.* Thiolactomycin and related analogues as novel anti-
831 mycobacterial agents targeting KasA and KasB condensing enzymes in
832 *Mycobacterium tuberculosis*. *J. Biol. Chem.* **275**, 16857-16864 (2000).
833 20 Cantaloube, S., Veyron-Churlet, R., Haddache, N., Daffe, M. & Zerbib, D.
834 The *Mycobacterium tuberculosis* FAS-II dehydratases and methyltransferases
835 define the specificity of the mycolic acid elongation complexes. *PloS One* **6**,
836 e29564 (2011).
837 21 Bahnson, B. J., Anderson, V. E. & Petsko, G. A. Structural mechanism of
838 enoyl-CoA hydratase: three atoms from a single water are added in either an
839 E1cb stepwise or concerted fashion. *Biochemistry* **41**, 2621-2629 (2002).
840 22 Rullas, J. *et al.* Fast standardized therapeutic-efficacy assay for drug discovery
841 against tuberculosis. *Antimicrob. Agents Chemother.* **54**, 2262-2264 (2010).
842 23 Engel, C. K., Mathieu, M., Zeelen, J. P., Hiltunen, J. K. & Wierenga, R. K.
843 Crystal structure of enoyl-coenzyme A (CoA) hydratase at 2.5 angstroms
844 resolution: a spiral fold defines the CoA-binding pocket. *EMBO J.* **15**, 5135-
845 5145 (1996).
846 24 Hamed, R. B., Batchelar, E. T., Clifton, I. J. & Schofield, C. J. Mechanisms
847 and structures of crotonase superfamily enzymes-how nature controls enolate
848 and oxyanion reactivity. *Cell. Mol. Life Sci.* **65**, 2507-2527 (2008).
849 25 Holm, L. & Rosenstrom, P. Dali server: conservation mapping in 3D. *Nucleic*
850 *Acids Res.* **38**, W545-549 (2010).

851 26 Hazbon, M. H. *et al.* Population genetics study of isoniazid resistance
852 mutations and evolution of multidrug-resistant *Mycobacterium tuberculosis*.
853 *Antimicrob. Agents Chemother.* **50**, 2640-2649 (2006).
854 27 Cole, S. T. *et al.* Massive gene decay in the leprosy bacillus. *Nature* **409**,
855 1007-1011 (2001).
856 28 Sassetti, C. M., Boyd, D. H. & Rubin, E. J. Genes required for mycobacterial
857 growth defined by high density mutagenesis. *Mol. Microbiol.* **48**, 77-84
858 (2003).
859 29 Franceschini, A. *et al.* STRING v9.1: protein-protein interaction networks,
860 with increased coverage and integration. *Nucleic Acids Res.* **41**, D808-815
861 (2013).
862 30 Kremer, L. *et al.* Mycolic acid biosynthesis and enzymic characterization of
863 the beta-ketoacyl-ACP synthase A-condensing enzyme from *Mycobacterium*
864 *tuberculosis*. *Biochem. J.* **364**, 423-430 (2002).
865 31 Besra, G. S. *et al.* Identification of the apparent carrier in mycolic acid
866 synthesis. *Proc. Natl. Acad. Sci. USA* **91**, 12735-12739 (1994).
867 32 Hu, Y. *et al.* 3-Ketosteroid 9alpha-hydroxylase is an essential factor in the
868 pathogenesis of *Mycobacterium tuberculosis*. *Mol. Microbiol.* **75**, 107-121
869 (2010).
870 33 Karimova, G., Pidoux, J., Ullmann, A. & Ladant, D. A bacterial two-hybrid
871 system based on a reconstituted signal transduction pathway. *Proc. Natl.*
872 *Acad. Sci. USA* **95**, 5752-5756 (1998).
873 34 Savitski, M. M. *et al.* Targeted data acquisition for improved reproducibility
874 and robustness of proteomic mass spectrometry assays. *J. Am. Soc. Mass*
875 *Spectrom.* **21**, 1668-1679 (2010).

876 35 Savitski, M. M. *et al.* Measuring and managing ratio compression for accurate
877 iTRAQ/TMT quantification. *J. Proteome Res.* **12**, 3586-3598 (2013).
878 36 Savitski, M. M. *et al.* Delayed fragmentation and optimized isolation width
879 settings for improvement of protein identification and accuracy of isobaric
880 mass tag quantification on Orbitrap-type mass spectrometers. *Anal. Chem.* **83**
881 8959-8967 (2011).
882 37 Kabsch, W. Xds. *Acta Crystallogr. D Biol. Crystallogr* **66**, 125-132 (2010).
883 38 CCP4. The CCP4 suite: programs for protein crystallography. *Acta*
884 *Crystallogr. D Biol. Crystallogr.* **50**, 760-763 (1994).
885 39 McCoy, A. J. *et al.* Phaser crystallographic software. *J. Appl. Crystallogr.* **40**,
886 658-674 (2007).
887 40 Emsley, P., Lohkamp, B., Scott, W. G. & Cowtan, K. Features and
888 development of Coot. *Acta Crystallogr. D Biol. Crystallogr.* **66**, 486-501,
889 (2010).
890 41 Murshudov, G. N., Vagin, A. A. & Dodson, E. J. Refinement of
891 macromolecular structures by the maximum-likelihood method. *Acta*
892 *Crystallogr. D Biol. Crystallogr.* **53**, 240-255 (1997).
893 42 Adams, P. D. *et al.* PHENIX: building new software for automated
894 crystallographic structure determination. *Acta Crystallogr. D Biol.*
895 *Crystallogr.* **58**, 1948-1954 (2002).
896
897

THPP target assignment reveals EchA6 as an essential fatty acid shuttle in mycobacteria

Supplementary Information Guide

Supplementary Figure 1. Essentiality of *echA6*, resistance and sensitivity to GSK951A *via echA6* and *mmpL3* overexpression in *M. bovis* BCG. (PDF, 1.3 MB) (**a,b**) Growth curves of Δ*BCG0957* in liquid medium with or without ATc (*n* = 2 biological replicates). One culture of Δ*BCG0957* was labeled with [^{14}C]-acetate at day 15 indicated by the arrow on panel *a* for 24 hours with the corresponding total MAMES and FAMES isolated, and equal counts for each sample subjected to TLC and exposed to Kodak X-Omat film as shown in panel *b* (*n* = 1 technical replicate). The second culture was monitored until cell lysis was observed and is shown in the inset of panel *a* (*n* = 1 technical replicate). (**c,d**) [^{14}C]-Acetate labeling of *M. bovis* BCG pVV16 and pVV16-*echA6* strains (*n* = 4 biological replicates). The corresponding total MAMES and FAMES were isolated and equal counts were subjected to either TLC (*c*, left panel) or reverse-phase TLC (panel *d*) and exposed to Kodak X-Omat film (*n* = 1 technical replicate). Cell wall bound MAMES were isolated from *M. bovis* BCG pVV16 and pVV16-*echA6* strains treated with GSK951A at 0.32 μM (1 × MIC, *c*, right panel, *n* = 4 biological replicates, 1 technical replicate) and equal volumes subjected to TLC and exposed to Kodak X-Omat film. (**e**) MIC determination of GSK951A against *M. bovis* BCG pVV16 and pVV16-*echA6* strains in liquid medium. (**f**) GSK951A sensitivity of *M. bovis* BCG pMV261 and pMV261-*mmpL3* strains in liquid medium. It should be noted that the plasmids pVV16 and pMV261 used in panels *e* and *f* have different antibiotic selection markers, kanamycin

26 and apramycin respectively, and hence have different synergy levels with THPPs. A
27 plasmid control is always used to give a base-line MIC for THPPs in plasmid-borne
28 overexpression studies.
29
30 **Supplementary Figure 2. Synthesis of total MAMES and FAMES, and cell wall**
31 **bound MAMES in the presence of GSK951A, GSK540A and MmpL3 inhibitors**.
32 (PDF, 2.2 MB)
33 [^{14}C]-Acetate labeling and dose-response of GSK951A, GSK540A, BM212 and
34 SQ109 on the synthesis of FAMES and MAMES (left panel), and cell wall bound
35 MAMES (centre panel) in *M. bovis* BCG. The corresponding total FAMES and
36 MAMES, and cell wall bound MAMES were isolated, and equal counts for the former
37 and equal volumes for the latter were subjected to TLC or reverse-phase TLC
38 (GSK951A, right panel) and exposed to Kodak X-Omat film. The corresponding
39 structures of GSK540A, BM212 and SQ109 are shown.
40
41 **Supplementary Figure 3. Lipid-[^{14}C]-labeling experiments using GSK951A**.
42 (PDF, 4.9 MB)
43 2D-TLC lipid profiles of *M. bovis* BCG (control) and GSK951A treated *M. bovis*
44 BCG (1 × and 4 × MIC). Apolar and polar lipids were isolated, and equal counts for
45 each sample subjected to TLC in solvent systems A to D1 (apolar lipids) and D2
46 (polar lipids), and exposed to Kodak X-Omat film. PDIMs, phthiocerol
47 dimycocerosates; TAG, triacylglycerol; MAT, multi-acylated trehaloses; F, fatty
48 acids; GroM, monomycolylglycerol; PGL, phenolic glycolipid; GMM, glucose
49 monomycolate; TMM, trehalose monomycolate.
50

51 **Supplementary Figure 4**. **Structural comparison of EchA6, evidence for binding**
52 **of GSK951A, and comparison of the mode of binding between THPP**
53 **compounds.** (PDF, 549 KB)
54 (**a**) Superposition of the EchA6 monomer (rainbow colored – N-terminal blue, C-
55 terminal red) and *Rattus norvegicus* enoyl-CoA hydratase (RnECH, grey ribbon, PDB
56 entry 1DUB[23]). (**b**) Superposition of the active sites of RnECH (1DUB, cyan stick
57 model) and *M. tuberculosis* EchA8 (3PZK, grey sticks). (**c**) Stereo diagram of
58 unbiased Fo-Fc density (contour level 3.0 σ) of C_{20}-CoA in molecule B of the
59 EchA6:C_{20}-CoA complex. Phases were from the initial refinement of the molecular
60 replacement solution for this complex, prior to incorporation of the ligand in the
61 structural model. (**d**) Stereo diagram of unbiased Fo-Fc density (contour level 2.5 σ)
62 of GSK951A in molecule B of the EchA6 trimer, calculated using model phases prior
63 to incorporation of the ligand model in the coordinates and amplitudes of the
64 EchA6:GSK951A complex. (**e-g**) Superposition of GSK951A with THPP compounds
65 GSK059A (*e*), GSK366A (*f*) and GSK572A (*g*). GSK059A lacks the trifluoromethyl
66 group and has a methyl instead. (**h**) Unbiased Fo-Fc density (contour level 3.0 σ) of
67 the bait compound GSK729A, calculated with model phases prior to incorporation of
68 the ligand in the coordinates and structure factor amplitudes of the EchA6:GSK729A
69 complex. Color coding of atoms: N, dark blue; O, red; F, pale cyan. Carbon atoms are
70 colored according to inhibitor: GSK951A, cyan; GSK366A, grey; GSK059A, green;
71 GSK572A, orange.
72
73 **Supplementary Figure 5. Predicted functional partners of EchA6 based on**
74 **database mining by STRING[29].** (PDF, 1.0 MB)

75 (**a**) Interaction network for EchA6 of *M. tuberculosis* H37Rv. FadB2 and FadB3, 3-
76 hydroxybutyryl-CoA dehydrogenases; FadB, fatty oxidation protein; FadD11, fatty
77 acid-CoA ligase; AccBC, acetyl-/propionyl-CoA carboxylase β-subunit; FadE5,
78 FadE15, FadE24, FadE25 and FadE36, acyl-CoA dehydrogenases. (**b**) Interaction
79 network for EchA6 of *M. leprae* Br4923. B1306.06c, 3-hydroxyisobutyryl-CoA
80 hydrolase; FadE23, putative acyl-CoA dehydrogenases; FadA and FadA4, acetyl-CoA
81 acetyltransferases; EftB, electron transfer flavoprotein β-subunit. All other proteins as
82 in panel *a*. Connecting lines are color coded as follows: green, genome
83 neighbourhood; red, gene fusion; blue, co-occurrence; black, co-expression;
84 turquoise, databases; yellow-green, text mining.
85
86 **Supplementary Figure 6**. **Original scans for all Western and TLC data.** (PDF, 8.8
87 MB)
88
89 **Supplementary Table 1. 6-plexed Chemoproteomics Experiment #1** (.xlsx, 225
90 KB)
91
92 **Supplementary Table 2. 6-plexed Chemoproteomics Experiment #2** (.xlsx, 193
93 KB)
94
95 **Supplementary Table 3. 6-plexed Chemoproteomics Experiment #3** (.xlsx, 184
96 KB)
97
98 **Supplementary Table 4. Ligand binding for EchA6 and EchA6^{W133A} probed by**
99 **intrinsic tryptophan fluorescence.** (PDF, 75.0 KB)

100 N.D. – not determined due to failure of non-linear fitting

101

102 **Supplementary Table 5. Crystallographic data and refinement statistics.** (PDF,

103 88.0 KB)

104 [1)] Values in parenthesis refer to the high resolution shell. [2)] The Ramachandran plot

105 distribution was calculated using Molprobity.

106

107 **Supplementary Table 6. EchA paralogues across mycobacterial genomes.** (PDF,

108 78.0 KB)

109 [1)] EchA paralogues with conserved catalytic carboxylates required for enoyl-CoA

110 hydratases activity in bold.

111

112 **Supplementary Table 7. The primers used in this study.** (PDF, 51.0 KB)

113

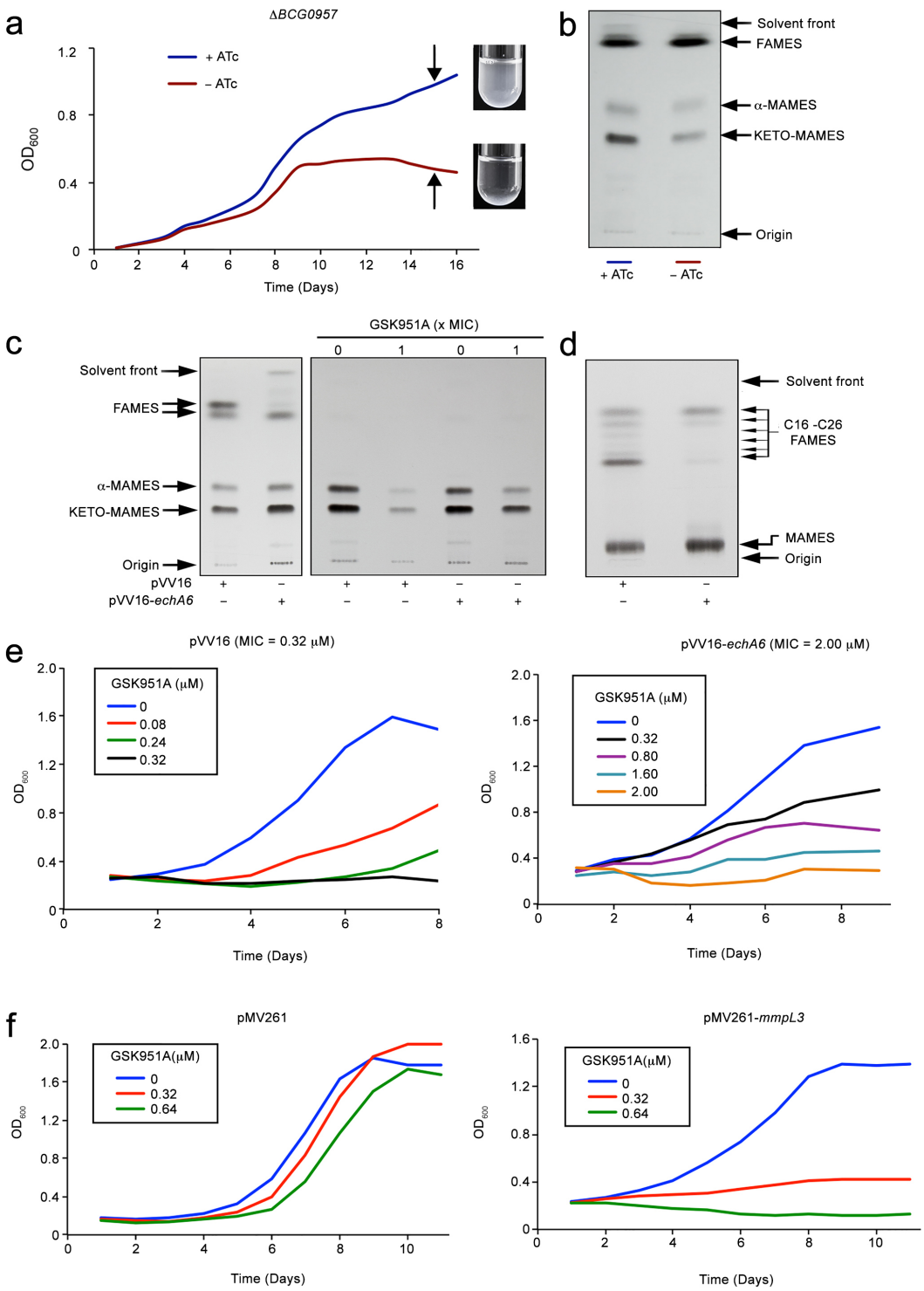
a
ΔBCG0957
+ ATc
– ATc
OD600
Time (Days)
b
Solvent front
FAMES
α-MAMES
KETO-MAMES
Origin
+ ATc
– ATc
c
GSK951A (x MIC)
0
1
0
1
Solvent front
FAMES
α-MAMES
KETO-MAMES
Origin
pVV16
pVV16-echA6
d
Solvent front
C16 -C26
FAMES
MAMES
Origin
e
pVV16 (MIC = 0.32 μM)
GSK951A (μM)
0
0.08
0.24
0.32
OD600
Time (Days)
pVV16-echA6 (MIC = 2.00 μM)
GSK951A (μM)
0
0.32
0.80
1.60
2.00
OD600
Time (Days)
f
pMV261
GSK951A(μM)
0
0.32
0.64
OD600
Time (Days)
pMV261-mmpL3
GSK951A(μM)
0
0.32
0.64
OD600
Time (Days)

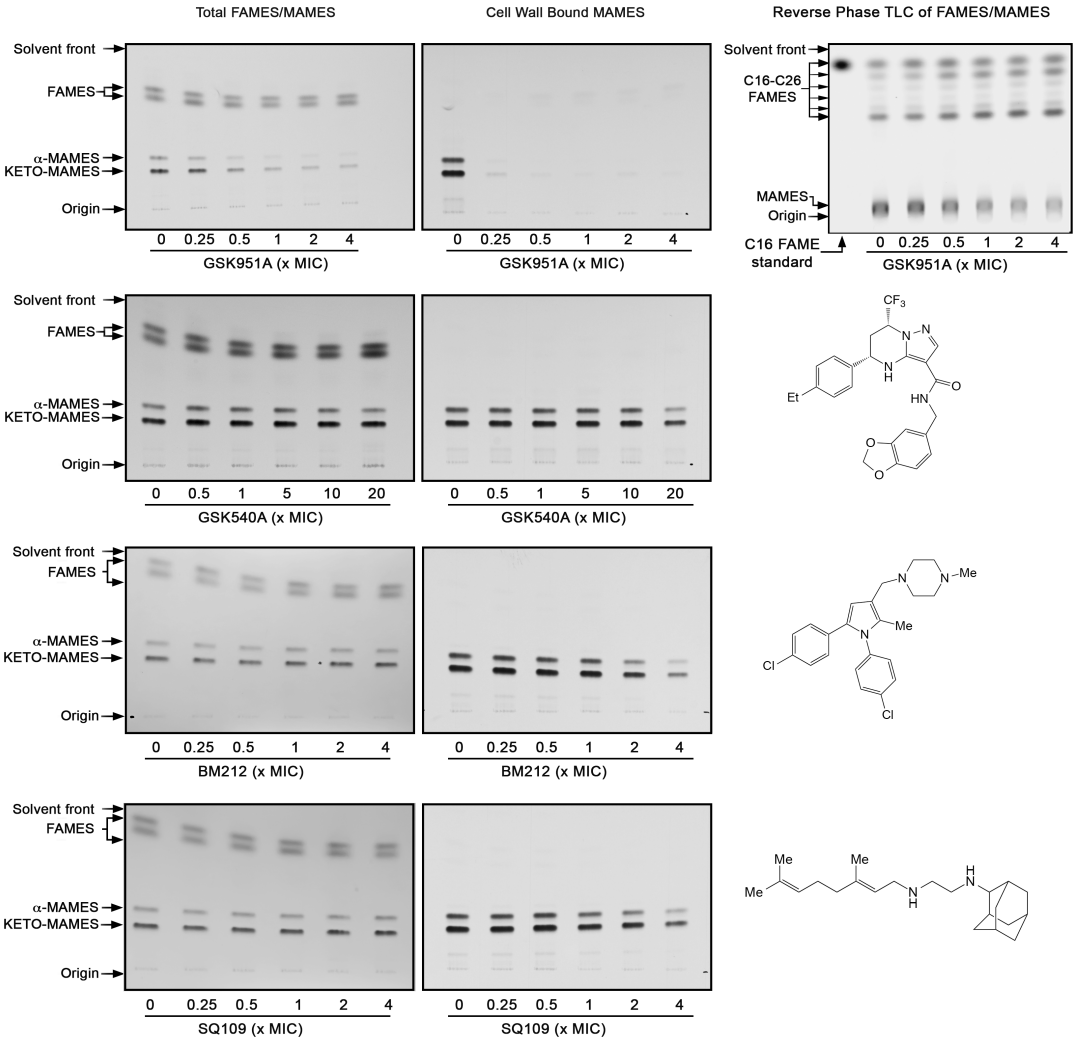
Total FAMES/MAMES
Cell Wall Bound MAMES
Reverse Phase TLC of FAMES/MAMES
Solvent front
FAMES
α-MAMES
KETO-MAMES
Origin
C16-C26 FAMES
MAMES
C16 FAME standard
0 0.25 0.5 1 2 4
GSK951A (x MIC)
0 0.5 1 5 10 20
GSK540A (x MIC)
BM212 (x MIC)
SQ109 (x MIC)
CF3
Et
HN
O
Me
Cl

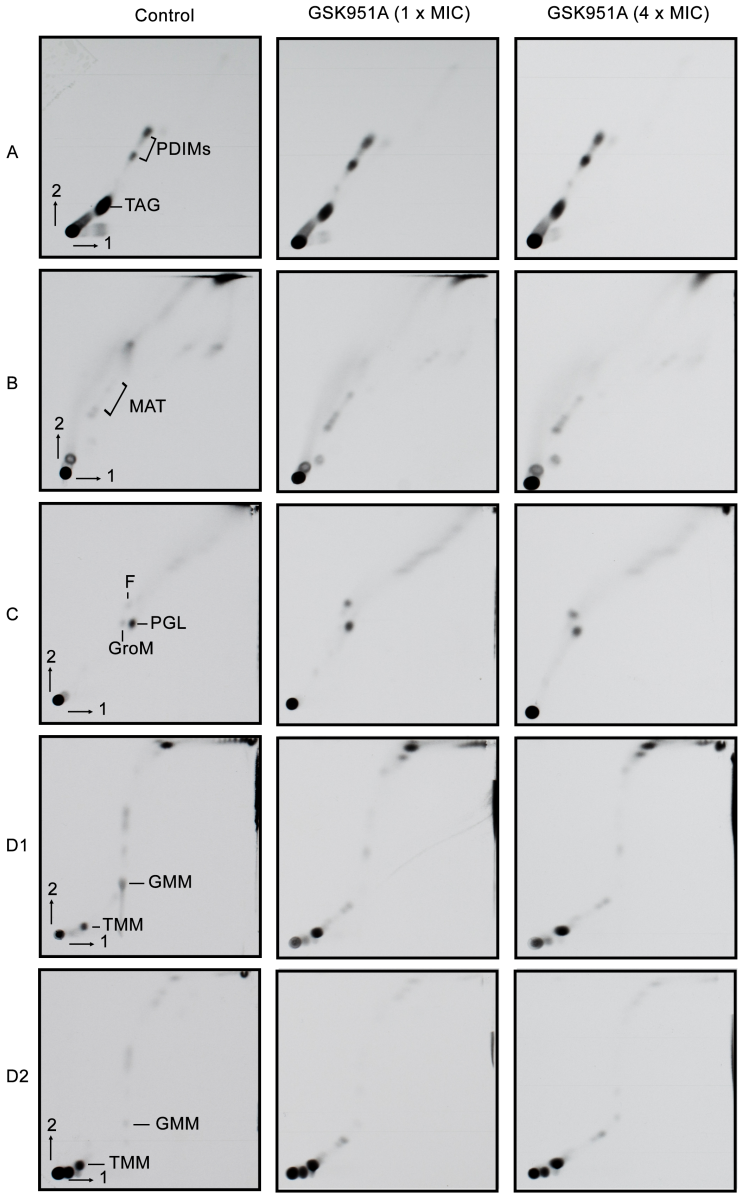
Control
GSK951A (1 x MIC)
GSK951A (4 x MIC)
A
PDIMs
TAG
2
1
B
MAT
2
1
C
F
PGL
GroM
2
1
D1
GMM
TMM
2
1
D2
GMM
TMM
2
1

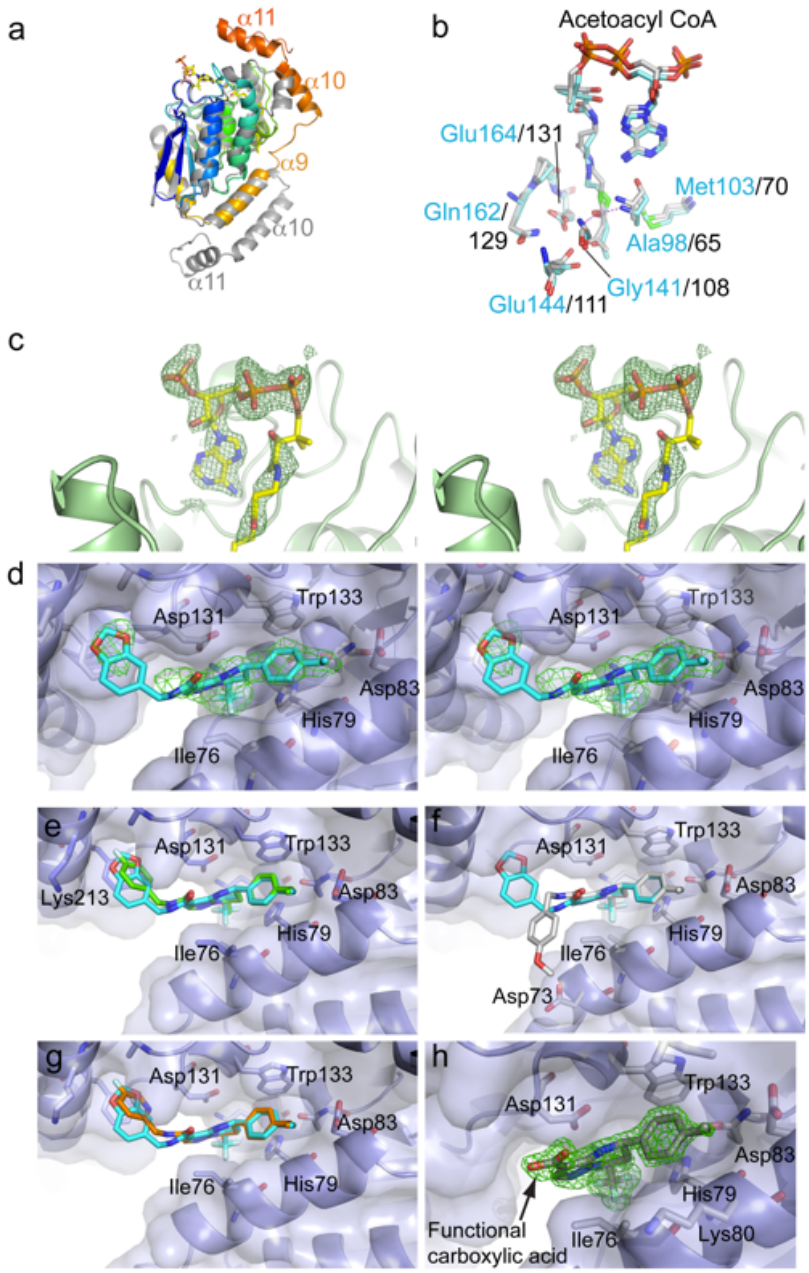
a
α11
α10
α9
α10
α11
b
Acetoacyl CoA
Glu164/131
Met103/70
Gln162/
129
Ala98/65
Gly141/108
Glu144/111
c
d
Trp133
Asp131
Asp83
His79
Ile76
e
Asp131
Trp133
Lys213
Asp83
His79
Ile76
f
Asp131
Trp133
Asp83
His79
Ile76
Asp73
g
Asp131
Trp133
Asp83
Ile76
His79
h
Trp133
Asp131
Asp83
His79
Functional
carboxylic acid
Ile76
Lys80

a

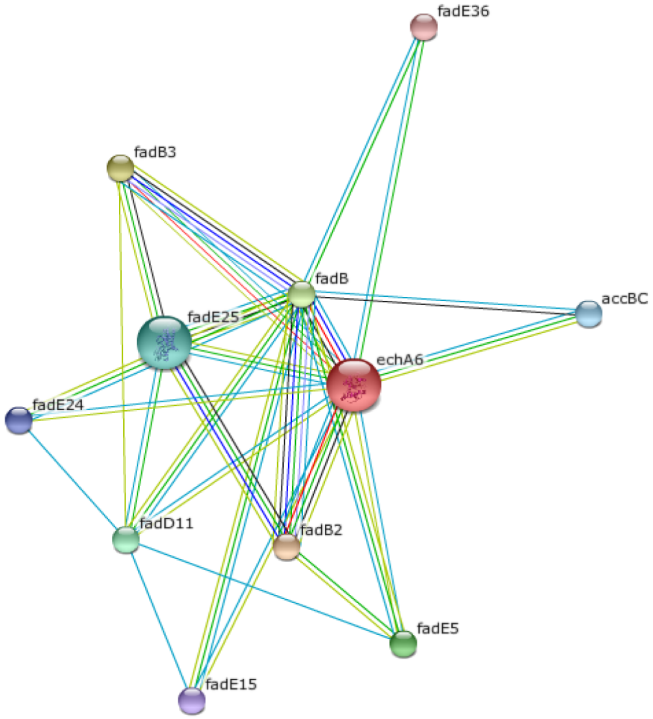
fadE36
fadB3
fadB
accBC
fadE25
echA6
fadE24
fadD11
fadB2
fadE5
fadE15

b

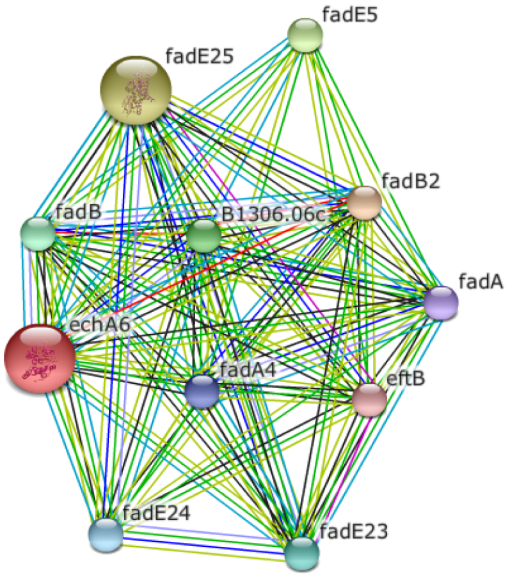
fadE5
fadE25
fadB2
fadB
B1306.06c
fadA
echA6
fadA4
eftB
fadE24
fadE23

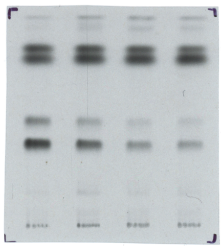

Figure 3a
(left panel)

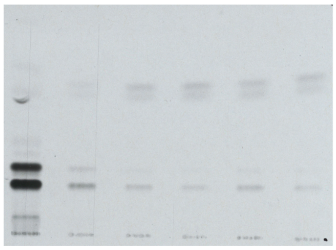

Figure 3a (middle panel)
Supplementary Figure 2
GSK951A (middle panel)

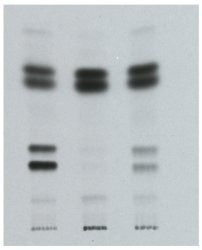

Figure 3a
(right panel)

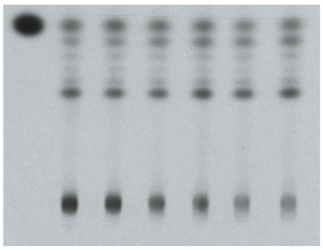

Figure 3b
Supplementary Figure 2
GSK951A (right panel)

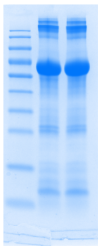

Figure 3c
(left panel)

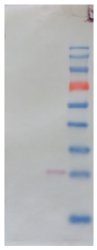

Figure 3c
(right panel)

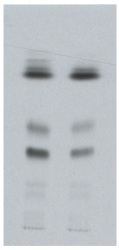

Supplementary
Figure 1b

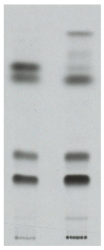

Supplementary
Figure 1c
(left panel)

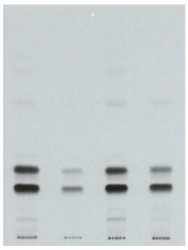

Supplementary
Figure 1c
(right panel)

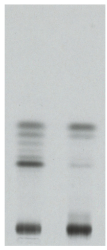

Supplementary
Figure 1d

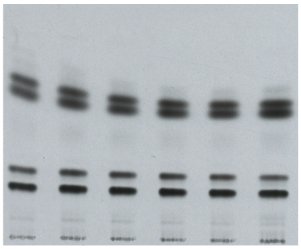

Supplementary Figure 2
GSK540A (left panel)

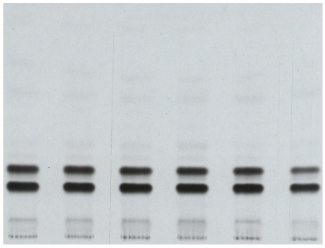

Supplementary Figure 2
GSK540A (right panel)

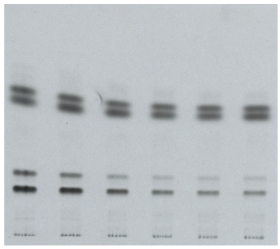

Supplementary Figure 2
GSK951A (left panel)

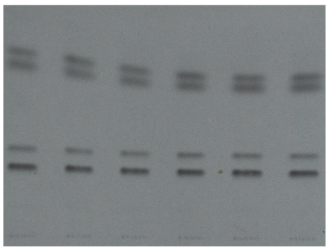

Supplementary Figure 2
BM212 (left panel)

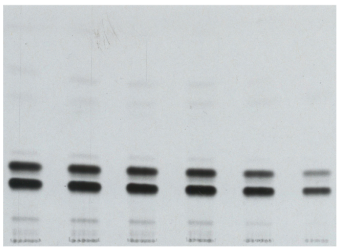

Supplementary Figure 2
BM212 (right panel)

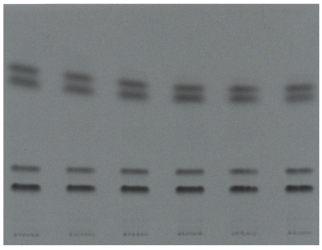

Supplementary Figure 2
SQ109 (left panel)

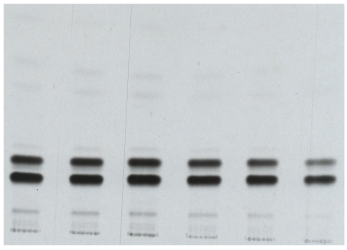

Supplementary Figure 2
SQ109 (right panel)

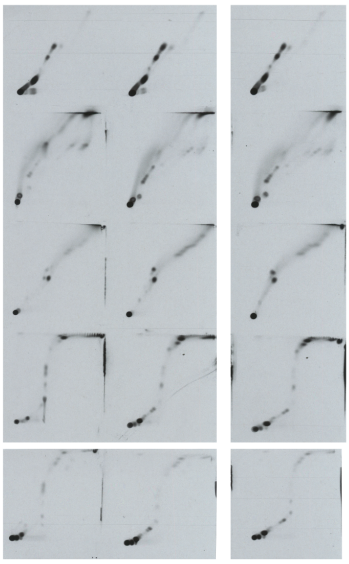

Supplementary Figure 3

Supplementary Table 2:
6-plexed Chemoproteomics Experiment #2

						sample 1 immobilized cpd: GSK729, 0.05 mM		sample 2 immobilized cpd: GSK729, 0.05 mM (replicate of sample 1)		sample 3 immobilized cpd: GSK729, 0.05 mM rebinding of nonbound fraction from sample 1		sample 3 immobilized cpd: GSK729, 0.05 mM rebinding of nonbound fraction from sample 2		sample 5 immobilized cpd: GSK729, 0.05 mM competing cpd: GSK729 100 µM		sample 6 immobilized cpd: GSK729, 0.05 mM competing cpd: GSK729 10 µM	
Name	**Protein description**	**MW**	**no_of_Quant. Spectra**	**no_of_Quant. Uniq. Peptides**	**fold change vs sample 6**	**sum ion area**	**peptides**	**fold change vs sample 6**	**sum ion area**	**peptides**	**fold change vs sample 6**	**sum ion area**	**peptides**	**fold change vs sample 6**	**sum ion area**	**peptides**	**fold change vs sample 6**	**sum ion area**	**peptides**
BCG_0957	PUTATIVE ENOYL-COA HYDRATASE ECHA6	26029	112	25	3.3	584,436,170	340	4.4	779,484,564	340	3.62	640,389,271	340	4.03	713,406,153	340	0.19	34,856,268	340
BCG_0717	DNA-DIRECTED RNA POLYMERASE (BETA' CHAIN)	146710	42	40	0.81	115,893,702	77	0.87	124,513,275	77	0.66	94,378,346	77	0.9	129,054,177	77	1.17	167,282,340	77
BCG_2801C	BIFUNCTIONAL PROTEIN POLYRIBONUCLEOTIDE	79735	33	25	0.87	147,364,550	60	0.84	143,354,793	60	0.76	129,221,064	60	0.77	130,357,722	60	0.99	168,159,585	60
BCG_0716	DNA-DIRECTED RNA POLYMERASE SUBUNIT BETA	129236	28	25	0.92	99,227,571	55	0.84	90,077,159	55	0.7	74,775,026	55	0.9	95,828,154	55	1.13	120,927,401	55
BCG_0956C	PUTATIVE ACETYL-COENZYME A CARBOXYLASE (	51772	17	17	0.94	44,883,476	31	1.29	61,734,500	31	0.75	35,753,984	31	0.9	42,798,433	31	1	47,836,684	31
BCG_3522C	PUTATIVE DNA-DIRECTED RNA POLYMERASE (ALI	37706	16	13	0.91	74,985,115	32	0.99	80,420,382	32	0.89	72,501,204	32	0.96	78,128,799	32	1.03	84,533,163	32
BCG_3523C	PUTATIVE 30S RIBOSOMAL PROTEIN S4 RPSD	23476	15	12	0.89	93,779,223	21	1.06	111,235,028	21	0.92	97,329,662	21	1.02	107,288,242	21	1.03	108,809,481	21
BCG_0389	PUTATIVE CHAPERONE PROTEIN DNAK	66831	14	14	0.72	31,682,011	34	1.08	47,162,829	34	0.91	39,628,293	34	0.93	40,890,426	34	0.86	38,086,016	34
BCG_1812C	HYPOTHETICAL INTEGRAL MEMBRANE PROTEIN	63512	14	14	0.74	25,729,976	31	0.94	32,552,596	31	0.81	27,994,773	31	0.92	31,924,698	31	1	34,756,593	31
BCG_2464C	PUTATIVE RIBONUCLEASE E RNE	103390	13	11	1.16	28,300,383	28	1.15	28,226,678	28	0.93	22,680,779	28	0.99	24,389,859	28	1.41	34,361,847	28
BCG_1357	PUTATIVE TRANSCRIPTION TERMINATION FACTO	65133	12	12	0.68	19,876,895	32	0.67	19,644,476	32	0.65	18,978,875	32	0.78	22,865,620	32	1.11	32,777,350	32
BCG_1668	PUTATIVE RIBOSOMAL PROTEIN S1 RPSA	53232	12	9	0.67	31,267,981	24	0.94	44,262,614	24	0.98	46,213,597	24	0.85	39,405,984	24	1.13	52,580,500	24
BCG_0437C	PUTATIVE ACYL-COA DEHYDROGENASE FADE7	42297	11	9	0.85	72,867,895	16	1.01	86,587,245	16	0.87	74,909,461	16	1.21	103,918,626	16	0.99	85,183,072	16
BCG_3007C	PUTATIVE DNA-BINDING PROTEIN HU HOMOLOG	21292	10	6	1.72	154,913,920	20	1.24	111,374,044	20	0.85	76,428,523	20	1.14	102,188,980	20	1.17	104,899,060	20
BCG_3238	PUTATIVE ATP-DEPENDENT RNA HELICASE RHLE	56703	10	10	0.92	27,581,006	17	1.01	29,995,584	17	0.95	28,532,792	17	0.99	29,450,561	17	1.37	40,982,989	17
BCG_3524C	PUTATIVE 30S RIBOSOMAL PROTEIN S11 RPSK	14771	8	6	1.02	74,808,931	13	1.11	81,029,220	13	1.01	74,437,798	13	1.3	95,093,512	13	1.21	88,657,921	13
BCG_0757	PUTATIVE 30S RIBOSOMAL PROTEIN S3 RPSC	30020	8	8	1	25,777,222	22	1.44	38,198,563	22	1.35	34,856,935	22	1.69	44,077,197	22	1.43	36,857,830	22
BCG_3488C	10 KDA CHAPERONIN GROES	10804	8	8	1.98	82,438,220	9	2.37	99,127,695	9	1.42	59,145,809	9	1.35	55,864,346	9	1.82	75,887,902	9
BCG_2859C	PUTATIVE TRANSLATION INITIATION FACTOR IF-2	94041	8	7	1.05	17,392,180	23	1.04	17,080,778	23	0.95	15,553,029	23	1.47	24,267,357	23	1.85	30,516,723	23
BCG_0479	60 KDA CHAPERONIN 2 GROEL2	56727	7	7	0.56	18,020,223	29	0.59	18,975,455	29	0.51	16,217,551	29	0.87	27,753,061	29	1.14	36,644,112	29
BCG_2447	ALKYL HYDROPEROXIDE REDUCTASE C PROTEIN	21566	6	6	1.05	22,048,865	17	1.13	23,606,614	17	1.02	21,412,938	17	1.08	22,667,928	17	0.89	18,483,061	17
BCG_0690	PUTATIVE 50S RIBOSOMAL PROTEIN L1 RPLA	24726	6	4	0.89	8,981,629	13	1.27	12,812,919	13	0.8	8,113,995	13	1.19	11,947,352	13	0.91	9,142,272	13
BCG_0280C	PUTATIVE 3-OXOACYL-ACYL-CARRIER PROTEIN)	46830	6	6	0.88	11,046,936	10	0.55	6,842,445	10	0.43	5,353,855	10	1.19	15,035,912	10	1.04	13,043,185	10
BCG_0086	PUTATIVE 30S RIBOSOMAL PROTEIN S18-1 RPSR1	9543	6	6	1.12	28,873,213	10	0.97	24,303,134	10	0.87	22,231,972	10	1.41	36,359,363	10	1.15	29,035,572	10
BCG_0752	PUTATIVE 50S RIBOSOMAL PROTEIN L4 RPLD	23743	6	6	0.76	12,963,165	12	0.98	16,747,963	12	1.09	18,466,335	12	0.98	16,874,198	12	1.26	21,576,211	12
BCG_3269C	PUTATIVE PREPROTEIN TRANSLOCASE SUBUNIT	106022	6	6	1.04	5,991,307	16	0.8	4,667,807	16	0.82	4,707,328	16	1.04	5,998,369	16	1.31	7,652,388	16
BCG_3863C	PUTATIVE FATTY-ACID-COA LIGASE FADD32	69260	5	5	1	5,763,981	12	0.74	4,265,874	12	1.01	5,858,425	12	0.99	5,711,968	12	0.78	4,459,127	12
BCG_3008C	PUTATIVE 3-ISOPROPYLMALATE DEHYDRATASE S	21780	5	5	0.84	6,810,685	5	0.93	7,533,575	5	0.76	6,181,259	5	0.97	7,903,264	5	0.87	7,095,900	5
BCG_1595	PUTATIVE FATTY ACYL-COA REDUCTASE	36821	5	5	0.92	20,096,155	9	0.81	17,693,711	9	0.71	15,488,336	9	1.23	26,906,753	9	1.04	22,635,061	9
BCG_0516	HEPARIN BINDING HEMAGGLUTININ HBHA	21534	5	5	0.87	17,425,277	9	0.97	19,428,798	9	0.73	14,551,654	9	0.89	17,836,914	9	1.11	22,141,638	9
BCG_0780	HYPOTHETICAL PROTEIN	25980	5	5	1.07	13,375,046	9	1.29	16,089,333	9	0.8	10,012,397	9	1.15	14,373,935	9	1.18	14,776,931	9
BCG_3704C	DNA TOPOISOMERASE I TOPA	102370	5	5	1.08	12,079,166	26	1.11	12,184,585	26	0.82	9,230,913	26	1.02	11,376,411	26	1.22	13,679,046	26
BCG_1680	PUTATIVE INITIATION FACTOR IF-3 INFC	22349	5	5	1.06	16,060,497	10	0.78	11,867,874	10	0.84	12,705,926	10	1.11	16,778,180	10	1.3	19,706,601	10
BCG_3127C	PUTATIVE CELL DIVISION ATP-BINDING PROTEIN	25596	5	5	1.03	6,357,925	9	0.85	5,208,584	9	1.21	7,477,020	9	1.35	8,289,120	9	1.41	8,664,997	9
BCG_0084	PUTATIVE 30S RIBOSOMAL PROTEIN S6 RPSF	10935	4	4	0.85	2,489,221	7	1.38	4,016,916	7	0.69	1,997,838	7	1.42	4,130,902	7	0.84	2,451,107	7
BCG_3662C	PUTATIVE LSR2 PROTEIN PRECURSOR	12098	4	4	0.99	4,728,361	10	0.85	4,058,255	10	1.06	5,080,533	10	1.15	5,508,663	10	0.89	4,282,565	10
BCG_3904	PUTATIVE BACTERIOFERRITIN BFRB	20442	4	3	1	6,603,042	4	1.12	7,360,748	4	0.91	6,021,977	4	1.19	7,856,254	4	0.96	6,348,024	4
BCG_0750	30S RIBOSOMAL PROTEIN S10 RPSJ (TRANSCRIP	11431	4	3	1.23	13,129,480	7	1.07	11,404,262	7	0.95	10,130,186	7	1.19	12,771,723	7	1.05	11,231,300	7
BCG_0751	PUTATIVE 50S RIBOSOMAL PROTEIN L3 RPLC	23090	4	4	1.25	10,688,345	5	0.88	7,551,018	5	0.91	7,804,145	5	0.7	6,014,855	5	1.11	9,476,962	5
BCG_2911C	PUTATIVE 30S RIBOSOMAL PROTEIN S2 RPSB	31089	4	4	0.85	5,996,733	10	0.89	6,253,702	10	0.9	6,336,680	10	1.06	7,500,075	10	1.26	8,884,240	10
BCG_3853	PUTATIVE SHORT-CHAIN TYPE DEHYDROGENASE	27469	4	3	1.16	2,655,748	4	0.31	717,195	4	0.75	1,716,898	4	1.18	2,693,003	4	1.3	2,957,521	4
BCG_2243	HYPOTHETICAL PROTEIN	56332	4	4	1.67	2,713,499	7	1.84	2,996,500	7	0.42	678,269	7	1.78	2,892,943	7	1.56	2,538,273	7
BCG_1676	EXCINUCLEASE ABC, SUBUNIT A UVRA	106132	3	3	0.19	380,243	10	0.68	1,338,692	10	0.27	538,015	10	0.38	747,802	10	0.32	627,849	10
BCG_0504C	HYPOTHETICAL PROTEIN	21305	3	3	1.01	9,633,368	3	0.63	5,985,824	3	0.82	7,801,373	3	1.36	12,957,745	3	0.77	7,400,899	3
BCG_2768C	HYPOTHETICAL PROTEIN	59532	3	3	0.72	8,076,259	3	0.8	9,027,629	3	0.54	6,096,935	3	0.82	9,177,268	3	0.94	10,604,054	3
BCG_0183	PUTATIVE ALDEHYDE DEHYDROGENASE (NAD+)	55035	3	3	0.62	3,569,500	13	1.07	6,110,749	13	0.88	5,034,746	13	0.73	4,150,407	13	0.95	5,452,738	13
BCG_3487C	60 KDA CHAPERONIN 1 GROEL1	55877	3	3	0.84	3,569,591	8	0.46	1,939,798	8	0.42	1,794,534	8	0.82	3,469,544	8	0.99	4,188,503	8
BCG_2962C	PUTATIVE MULTIFUNCTIONAL MYCOCEROSIC ACI	224396	3	3	0.71	4,148,478	11	1.13	6,549,409	11	0.53	3,108,438	11	0.87	5,045,389	11	1.02	5,941,255	11
BCG_3521C	PUTATIVE 50S RIBOSOMAL PROTEIN L17 RPLQ	19475	3	3	0.79	5,605,734	4	0.93	6,561,208	4	0.86	6,082,612	4	0.92	6,494,061	4	1.15	8,127,840	4
BCG_0767	PUTATIVE 30S RIBOSOMAL PROTEIN S14 RPSN1	6825	3	1	2.19	5,437,546	4	2.22	5,510,842	4	1.45	3,600,908	4	2.69	6,678,362	4	1.43	3,537,849	4
BCG_2607C	ADENINE PHOSPHORIBOSYLTRANSFERASE APT	23246	3	3	1.03	3,956,989	5	1.68	6,490,680	5	0.78	3,018,986	5	1.23	4,743,091	5	1.46	5,613,897	5
BCG_0771	PUTATIVE 30S RIBOSOMAL PROTEIN S5 RPSE	22888	3	3	1.73	22,420,008	12	1.09	14,100,508	12	0.96	12,473,539	12	1.43	18,442,270	12	1.8	23,258,977	12
BCG_2261	MEROMYCOLATE EXTENSION ACYL CARRIER PRO	12524	3	2	2.4	20,267,246	4	3.43	28,950,302	4	1.63	13,767,254	4	2.37	19,999,185	4	2.08	17,531,802	4
BCG_0023C	PUTATIVE CHROMOSOME PARTITIONING PROTEI	37018	2	2	0.95	1,717,706	8	0.62	1,134,293	8	0	0	8	1.82	3,304,326	8	0	0	8
BCG_0622	HYPOTHETICAL PROTEIN TB27 3	27343	2	2	0.87	866,042	3	0	0	3	2.52	2,523,344	3	0.93	935,754	3	0	0	3
BCG_0772	PUTATIVE 50S RIBOSOMAL PROTEIN L30 RPMD	7347	2	2	1.94	873,271	2	1.48	667,318	2	2.11	953,019	2	2.28	1,027,885	2	0	0	2
BCG_3270C	HYPOTHETICAL PROTEIN	24567	2	2	1.86	2,082,763	4	1.16	1,306,045	4	0.43	487,281	4	1.97	2,212,882	4	0	0	4
BCG_2183C	HYPOTHETICAL PROTEIN	15912	2	2	0.38	585,851	5	0.8	1,213,064	5	1.05	1,605,428	5	1.5	2,280,626	5	0.11	172,009	5
BCG_0770	PUTATIVE 50S RIBOSOMAL PROTEIN L18 RPLR	13184	2	2	0.65	5,269,742	4	0.69	5,581,176	4	0.7	5,693,091	4	0.69	5,598,605	4	0.51	4,112,493	4
BCG_0963	HYPOTHETICAL PROTEIN	27627	2	2	0.87	3,624,397	5	0.72	2,976,761	5	0.76	3,156,759	5	0.88	3,631,703	5	0.59	2,440,274	5
BCG_0701	PUTATIVE 50S RIBOSOMAL PROTEIN L7/L12 RPLL	13440	2	2	0.3	622,998	4	0.85	1,746,389	4	1.64	3,374,214	4	0.56	1,148,538	4	0.68	1,390,819	4
BCG_3009C	PUTATIVE 3-ISOPROPYLMALATE DEHYDRATASE L	50199	2	2	0.47	2,661,047	7	0.76	4,327,239	7	0.83	4,705,067	7	0.8	4,523,338	7	0.7	3,981,023	7
BCG_3915	PUTATIVE HISTONE-LIKE PROTEIN HNS	13823	2	2	0.84	3,553,100	2	0.87	3,664,132	2	0.72	3,042,144	2	1.02	4,299,548	2	0.81	3,429,665	2
BCG_3142	PUTATIVE THIOSULFATE SULFURTRANSFERASE (	35999	2	2	0.84	6,073,809	6	0.96	6,927,817	6	0.95	6,852,531	6	1.11	8,035,866	6	0.82	5,952,770	6
BCG_1798	PUTATIVE CUTINASE CUT1	21999	2	1	0.96	3,018,382	2	0.91	2,883,511	2	0.83	2,607,175	2	0.96	3,016,357	2	0.83	2,622,816	2
BCG_1964	PUTATIVE ACYL-COA LIGASE FADD31	66310	2	2	0.51	1,758,351	4	0.67	2,335,956	4	0.81	2,828,664	4	0.59	2,054,499	4	0.89	3,094,959	4
BCG_0734	PUTATIVE ELONGATION FACTOR TU TUF (EF-TU)	43594	2	2	0.69	4,453,905	4	0.65	4,205,096	4	0.55	3,534,045	4	0.27	1,766,358	4	1.05	6,811,165	4
BCG_2462C	PUTATIVE 50S RIBOSOMAL PROTEIN L21 RPLU	11151	2	2	0.5	3,544,106	2	0.69	4,878,585	2	1	7,070,810	2	0.87	6,091,105	2	1.14	8,039,184	2
BCG_1449	PUTATIVE INTEGRATION HOST FACTOR MIHF	20835	2	2	0.85	6,398,985	4	1.11	8,327,887	4	0.85	6,357,036	4	2.07	15,465,283	4	1.28	9,619,441	4
BCG_2017	HYPOTHETICAL PROTEIN	59895	2	2	0.99	1,210,970	5	1.27	1,550,028	5	0.53	648,510	5	1.31	1,602,316	5	1.61	1,963,596	5
BCG_0050C	HYPOTHETICAL PROTEIN TB39 8	56003	2	2	1.02	1,095,398	7	2.02	2,164,298	7	2.04	2,180,517	7	2.49	2,661,116	7	2.1	2,247,070	7
BCG_3118C	PUTATIVE OXIDOREDUCTASE	34649	2	2 n.d.		1,023,679	2 n.d.		0	2 n.d.		0	2 n.d.		750,346	2 n.d.		681,318	2 n.d.

Supplementary Table 1:
6-plexed Chemoproteomics Experiment #1

					sample 1 immobilized cpd: GSK729, 2mM competing cpd: GSK729 100 µM			sample 2 immobilized cpd: GSK729, 2mM competing cpd: GSK730, 100 µM				sample 3 immobilized cpd: GSK729, 2mM competing cpd: none			sample 4 immobilized cpd: GSK730, 2mM competing cpd: GSK729, 100 µM			sample 5 immobilized cpd: GSK730, 2mM competing cpd: GSK730 100 µM			sample 6 immobilized cpd: GSK730, 2mM competing cpd: none		
Name	**Protein description**	**MW**	**no_of_Quant. Spectra**	**no_of_Quant. Uniq. Peptides**	**fold change vs sample 3**	**sum ion area**	**peptides**	**fold change vs sample 3**	**sum ion area**	**peptides**	**fold change vs sample 6**	**fold change vs sample 3**	**sum ion area**	**peptides**	**fold change vs sample 6**	**sum ion area**	**peptides**	**fold change vs sample 6**	**sum ion area**	**peptides**	**fold change vs sample 6**	**sumionarea**	**peptides**
BCG_0957	PUTATIVE ENOYL-COA HYDRATASE ECHA6	26029	344	26	0.08	22,561,852	524	0.84	227,297,647	524	11.09	1	272,611,013	524	0.49	12,115,720	524	0.52	12,721,330	524	1	24,576,703	524
BCG_1367	PUTATIVE ATP SYNTHASE DELTA CHAIN ATPH	48806	2	1	0.58	32,943	4	0.46	26,093	4	2.27	1	57,247	4	1.16	29,111	4	1.95	49,022	4	1	25,192	4
BCG_3238	PUTATIVE ATP-DEPENDENT RNA HELICASE RHLE	56703	26	20	1.11	15,628,958	35	1.18	16,591,469	35	2.19	1	14,006,490	35	2.56	16,361,831	35	1.62	10,363,466	35	1	6,390,235	35
BCG_0963	HYPOTHETICAL PROTEIN	27627	3	3	0.87	1,816,722	3	1.81	3,794,322	3	2.06	1	2,091,866	3	0.31	312,711	3	2.05	2,079,214	3	1	1,015,038	3
BCG_2261	MEROMYCOLATE EXTENSION ACYL CARRIER PROTEI	12524	2	1	1.49	380,655	2	1.19	302,892	2	1.94	1	254,747	2	1.64	215,222	2	1.6	209,948	2	1	131,455	2
BCG_0751	PUTATIVE 50S RIBOSOMAL PROTEIN L3 RPLC	23090	15	12	1.4	10,675,857	18	1.48	11,327,314	18	1.89	1	7,623,841	18	2.44	9,878,390	18	1.64	6,625,638	18	1	4,039,291	18
BCG_3965	HYPOTHETICAL PROTEIN	27171	10	10	1.31	7,664,819	10	1.28	7,496,556	10	1.74	1	5,874,225	10	2.25	7,560,717	10	1.47	4,957,715	10	1	3,381,993	10
BCG_0760	PUTATIVE 50S RIBOSOMAL PROTEIN S17 RPSQ	14872	4	3	1.17	4,988,692	4	1.42	6,067,778	4	1.68	1	4,260,958	4	1.9	4,824,421	4	1.43	3,635,661	4	1	2,541,184	4
BCG_1313	PUTATIVE COLD-SHOCK DEAD-BOX PROTEIN A HOMC	61421	3	3	1.09	1,270,986	5	1.26	1,467,684	5	1.59	1	1,164,843	5	1.59	1,169,044	5	1.5	1,097,041	5	1	733,016	5
BCG_1624	HYPOTHETICAL PROTEIN	18100	4	4	1.03	1,953,733	7	0.98	1,861,725	7	1.58	1	1,898,355	7	1.53	1,835,953	7	1.5	1,800,512	7	1	1,200,192	7
BCG_2768C	HYPOTHETICAL PROTEIN	59532	10	10	0.84	7,837,771	10	0.79	7,356,198	10	1.52	1	9,350,016	10	1.38	8,399,679	10	1.05	6,416,461	10	1	6,137,718	10
BCG_3525C	PUTATIVE 30S RIBOSOMAL PROTEIN S13 RPSM	14351	21	17	1	18,260,366	33	1.09	20,013,882	33	1.52	1	18,195,430	33	1.5	17,986,864	33	1.17	13,992,606	33	1	11,960,179	33
BCG_2229	PUTATIVE AMINOPEPTIDASE PEPB	53447	4	4	0.76	2,332,491	6	0.78	2,387,504	6	1.42	1	3,050,887	6	1.4	3,018,078	6	0.99	2,123,093	6	1	2,155,107	6
BCG_3142	PUTATIVE THIOSULFATE SULFURTRANSFERASE CYS.	35999	4	4	0.79	2,740,714	8	0.63	2,167,615	8	1.41	1	3,451,566	8	1.16	2,825,778	8	1.86	4,543,703	8	1	2,440,123	8
BCG_2801C	BIFUNCTIONAL PROTEIN POLYRIBONUCLEOTIDE NUC	79735	79	43	0.91	52,271,945	116	0.82	46,871,956	116	1.41	1	57,568,748	116	1.3	52,870,601	116	1	40,815,704	116	1	40,756,167	116
BCG_0780	HYPOTHETICAL PROTEIN	25980	3	3	0.78	2,581,717	4	0.92	3,041,232	4	1.41	1	3,305,621	4	1.09	2,553,882	4	0.97	2,275,123	4	1	2,342,153	4
BCG_0437C	PUTATIVE ACYL-COA DEHYDROGENASE FADE7	42297	22	17	0.86	17,989,359	30	0.84	17,564,499	30	1.40	1	20,864,561	30	1.45	21,834,552	30	0.98	14,630,595	30	1	14,909,916	30
BCG_2464C	PUTATIVE RIBONUCLEASE E RNE	103390	38	32	1.47	38,754,206	55	1.11	29,323,055	55	1.38	1	26,506,052	55	1.76	33,801,397	55	1.34	25,693,060	55	1	19,230,559	55
BCG_2550	HYPOTHETICAL PROTEIN	50192	8	8	1.11	7,102,687	9	1.14	7,245,925	9	1.38	1	6,364,650	9	1.63	7,549,463	9	1.3	6,023,058	9	1	4,627,183	9
BCG_0689	PUTATIVE 50S RIBOSOMAL PROTEIN L11 RPLK	15003	12	11	0.98	10,898,148	12	1.07	12,002,970	12	1.37	1	11,189,280	12	1.14	9,342,310	12	1	8,210,883	12	1	8,175,776	12
BCG_3009C	PUTATIVE 3-ISOPROPYLMALATE DEHYDRATASE LAR(	50199	4	4	0.78	1,354,743	6	0.57	986,181	6	1.37	1	1,737,418	6	1.11	1,401,610	6	1	1,275,598	6	1	1,270,764	6
BCG_0956C	PUTATIVE ACETYL-COENZYME A CARBOXYLASE CAR	51772	18	14	0.92	8,997,565	23	0.89	8,679,435	23	1.35	1	9,727,810	23	1.43	10,291,475	23	1.03	7,394,628	23	1	7,190,980	23
BCG_0516	HEPARIN BINDING HEMAGGLUTININ HBHA	21534	5	5	1	6,010,458	9	1	6,026,653	9	1.35	1	6,024,311	9	1.49	6,630,503	9	1.23	5,524,738	9	1	4,457,046	9
BCG_2800C	PUTATIVE ZINC PROTEASE PEPR	47072	9	8	1.07	4,066,556	11	1.16	4,450,095	11	1.34	1	3,813,531	11	1.54	4,369,064	11	1.21	3,434,410	11	1	2,849,518	11
BCG_3904	PUTATIVE BACTERIOFERRITIN BFRB	20442	4	3	0.97	3,178,911	4	0.9	2,959,060	4	1.32	1	3,278,110	4	0.89	2,201,259	4	0.97	2,411,489	4	1	2,478,522	4
BCG_0389	PUTATIVE CHAPERONE PROTEIN DNAK	66831	22	19	0.92	26,642,757	42	0.73	21,230,793	42	1.32	1	28,963,178	42	1.12	24,670,358	42	1	21,974,176	42	1	21,988,061	42
BCG_0701	PUTATIVE 50S RIBOSOMAL PROTEIN L7/L12 RPLL (SA:	13440	9	8	1.22	11,697,068	10	1.28	12,130,847	10	1.30	1	9,557,224	10	1.04	7,598,097	10	1.22	9,019,248	10	1	7,332,765	10
BCG_3277C	PUTATIVE ADENOSYLHOMOCYSTEINASE SAHH	54324	5	5	1.44	5,432,753	9	0.94	3,555,292	9	1.30	1	3,787,110	9	0.92	2,679,529	9	1.18	3,435,480	9	1	2,923,280	9
BCG_0700	PUTATIVE 50S RIBOSOMAL PROTEIN L10 RPLJ	18478	13	12	1	12,412,153	17	1.15	14,206,782	17	1.29	1	12,327,374	17	1.04	9,951,194	17	0.96	9,115,494	17	1	9,545,845	17
BCG_1812C	HYPOTHETICAL INTEGRAL MEMBRANE PROTEIN	63512	40	28	0.91	21,765,889	49	0.79	18,959,698	49	1.29	1	23,862,901	49	1.2	22,297,962	49	1.18	22,275,268	49	1	18,565,322	49
BCG_0929	HYPOTHETICAL PROTEIN	27469	3	2	0.64	596,200	3	0.67	622,696	3	1.28	1	934,459	3	0.96	702,673	3	0.64	470,289	3	1	732,563	3
BCG_0773	PUTATIVE 50S RIBOSOMAL PROTEIN L15 RPLO	15521	8	8	1.49	6,540,582	12	1.34	5,930,384	12	1.25	1	4,316,657	12	1.6	5,579,746	12	1.17	4,095,609	12	1	3,451,596	12
BCG_2371C	PUTATIVE GLYCYL-TRNA SYNTHETASE GLYS	52938	13	12	0.81	9,965,212	20	0.87	10,709,397	20	1.24	1	12,315,657	20	1.15	11,435,330	20	1.01	9,943,903	20	1	9,897,397	20
BCG_2237	GLUTAMINE SYNTHETASE GLNA1	53570	4	4	1.19	4,614,839	7	1.02	3,925,938	7	1.24	1	3,864,811	7	0.97	3,027,127	7	1.12	3,486,681	7	1	3,116,077	7
BCG_0758	PUTATIVE 50S RIBOSOMAL PROTEIN L16 RPLP	15692	8	6	2.03	4,823,549	11	2.02	4,835,082	11	1.23	1	2,429,915	11	2.72	5,356,343	11	1.51	2,978,556	11	1	1,974,731	11
BCG_0732	PUTATIVE 30S RIBOSOMAL PROTEIN S7 RPSG	17600	18	16	1.02	13,841,494	28	1.13	15,580,505	28	1.23	1	13,751,663	28	1.16	12,937,735	28	0.92	10,208,127	28	1	11,196,927	28
BCG_2859C	PUTATIVE TRANSLATION INITIATION FACTOR IF-2 INFI	94041	25	24	1.23	22,066,124	38	1.06	18,863,769	38	1.22	1	17,870,667	38	1.51	21,972,264	38	1.33	19,411,761	38	1	14,610,322	38
BCG_0227	HYPOTHETICAL PROTEIN	10365	2	2	0.68	1,351,694	3	0.95	1,871,713	3	1.22	1	1,978,796	3	0.84	1,354,869	3	0.86	1,393,158	3	1	1,618,368	3
BCG_3508C	PUTATIVE 30S RIBOSOMAL PROTEIN S9 RPSI	16436	7	7	1.32	7,019,943	10	1.77	9,439,799	10	1.22	1	5,343,784	10	1.61	6,938,039	10	1.48	6,441,238	10	1	4,370,956	10
BCG_2461C	PUTATIVE 50S RIBOSOMAL PROTEIN L27 RPMA	8968	4	4	1.34	5,165,073	5	1.39	5,349,935	5	1.22	1	3,849,050	5	1.62	5,114,387	5	1.25	3,937,725	5	1	3,152,236	5
BCG_1357	PUTATIVE TRANSCRIPTION TERMINATION FACTOR RI	65133	24	20	0.94	16,545,771	31	0.87	15,381,229	31	1.22	1	17,528,236	31	1.14	16,332,870	31	1.03	14,682,035	31	1	14,406,138	31
BCG_3522C	PUTATIVE DNA-DIRECTED RNA POLYMERASE (ALPHA	37706	10	7	0.99	5,567,630	14	1.01	5,698,760	14	1.21	1	5,666,866	14	1.04	4,841,164	14	1.08	5,049,631	14	1	4,667,735	14
BCG_2744	HYPOTHETICAL ALANINE AND ARGININE RICH PROTE	49796	2	2	0.94	2,111,825	3	0.87	1,962,867	3	1.21	1	2,251,046	3	1.12	2,087,952	3	1.01	1,879,355	3	1	1,861,575	3
BCG_0753	PUTATIVE 50S RIBOSOMAL PROTEIN L23 RPLW	10958	8	7	1.09	4,724,966	10	1.35	5,816,545	10	1.21	1	4,315,111	10	1.26	4,490,710	10	1.13	4,036,410	10	1	3,573,696	10
BCG_0613	PUTATIVE CYTOCHROME P450 135B1 CYP135B1	50760	2	2	0.79	573,066	6	0.76	554,538	6	1.20	1	729,624	6	1.48	893,309	6	1.27	765,958	6	1	605,588	6
BCG_3118C	PUTATIVE OXIDOREDUCTASE	34649	4	3	0.56	564,190	5	0.88	880,386	5	1.20	1	1,000,700	5	0.85	706,057	5	0.75	627,091	5	1	832,315	5
BCG_0769	PUTATIVE 50S RIBOSOMAL PROTEIN L6 RPLF	19377	5	5	1.05	6,804,244	9	1.16	7,521,234	9	1.20	1	6,511,404	9	1.07	5,818,001	9	1.15	6,269,088	9	1	5,443,433	9
BCG_2112C	PUTATIVE ATP-DEPENDENT DNA HELICASE HELY	99636	20	18	1.05	12,919,583	29	0.85	10,365,290	29	1.19	1	12,292,147	29	1.2	12,330,655	29	0.97	9,950,431	29	1	10,305,243	29
BCG_2842C	HYPOTHETICAL PROTEIN	91047	2	2	0.86	1,319,639	8	0.73	1,119,643	8	1.18	1	1,538,531	8	0.97	1,256,390	8	0.95	1,239,447	8	1	1,300,814	8
BCG_2930C	PUTATIVE 30S RIBOSOMAL PROTEIN S16 RPSP	17437	5	4	1.37	2,044,595	8	1.71	2,587,541	8	1.17	1	1,506,379	8	1.49	1,907,296	8	1.69	2,160,949	8	1	1,288,521	8
BCG_1668	PUTATIVE RIBOSOMAL PROTEIN S1 RPSA	53232	39	30	0.96	36,075,789	45	0.86	32,301,446	45	1.17	1	37,782,860	45	1.1	35,579,990	45	1.01	32,665,919	45	1	32,346,561	45
BCG_0757	PUTATIVE 30S RIBOSOMAL PROTEIN S3 RPSC	30020	29	23	1.15	20,937,601	38	1.27	23,107,598	38	1.17	1	18,276,014	38	1.72	27,074,385	38	1.4	22,026,033	38	1	15,686,041	38
BCG_1947C	CATALASE-PEROXIDASE-PEROXYNITRITASE T KATG	80562	2	2	1.1	857,718	2	0.81	634,849	2	1.14	1	780,604	2	1.01	690,945	2	0.97	663,829	2	1	685,885	2
BCG_3008C	PUTATIVE 3-ISOPROPYLMALATE DEHYDRATASE SMA	21780	4	3	0.94	1,310,163	4	0.89	1,236,237	4	1.12	1	1,388,789	4	0.84	1,040,808	4	0.86	1,068,104	4	1	1,235,320	4
BCG_1676	EXCINUCLEASE ABC, SUBUNIT A UVRA	106132	17	15	0.98	10,811,474	20	0.81	8,941,967	20	1.12	1	11,071,180	20	1.31	12,922,185	20	1.03	10,187,747	20	1	9,879,593	20
BCG_2135C	PUTATIVE RNA METHYLTRANSFERASE	30123	6	6	1.45	6,509,639	6	1.36	6,069,361	6	1.11	1	4,487,631	6	1.54	6,231,228	6	1.24	4,991,770	6	1	4,041,563	6
BCG_0754	PUTATIVE 50S RIBOSOMAL PROTEIN L2 RPLB	30577	12	9	1.23	7,579,456	22	1.75	10,913,730	22	1.11	1	6,218,048	22	1.01	5,676,208	22	1.78	9,986,124	22	1	5,602,194	22
BCG_1389C	PUTATIVE GLUCANASE GLGE	78640	2	2	1.01	428,215	2	0.84	355,613	2	1.10	1	422,510	2	0.79	302,974	2	0.82	312,832	2	1	382,571	2
BCG_0690	PUTATIVE 50S RIBOSOMAL PROTEIN L1 RPLA	24726	20	15	1.14	19,793,695	24	1.14	19,737,280	24	1.09	1	17,238,732	24	1.22	19,331,895	24	1.01	16,057,050	24	1	15,837,968	24
BCG_3524C	PUTATIVE 30S RIBOSOMAL PROTEIN S11 RPSK	14771	7	6	0.83	6,671,248	9	1.15	9,280,505	9	1.09	1	8,170,040	9	1.29	9,607,126	9	1.08	8,097,439	9	1	7,507,668	9
BCG_3521C	PUTATIVE 50S RIBOSOMAL PROTEIN L17 RPLQ	19475	5	4	0.83	4,173,078	8	1	5,069,807	8	1.09	1	5,169,765	8	1.21	5,764,551	8	1.26	6,004,958	8	1	4,754,621	8
BCG_3704C	DNA TOPOISOMERASE I TOPA	102370	15	11	1.02	6,934,540	28	0.92	6,222,581	28	1.07	1	6,745,958	28	1.14	7,152,820	28	1.06	6,600,118	28	1	6,291,654	28
BCG_2843C	HYPOTHETICAL PROTEIN	34432	3	3	0.9	1,919,446	6	0.94	1,997,631	6	1.07	1	2,125,236	6	1.05	2,081,709	6	0.89	1,772,943	6	1	1,984,763	6
BCG_0510C	MYCOLIC ACID SYNTHASE PCAA	33028	2	2	0.97	1,665,742	3	0.69	1,175,984	3	1.07	1	1,709,125	3	1.1	1,757,500	3	0.92	1,475,331	3	1	1,597,138	3
BCG_2607C	ADENINE PHOSPHORIBOSYLTRANSFERASE APT	23246	4	4	1.08	3,257,115	5	1.2	3,638,814	5	1.07	1	3,023,967	5	1.54	4,359,919	5	1.3	3,668,330	5	1	2,831,654	5
BCG_0770	PUTATIVE 50S RIBOSOMAL PROTEIN L18 RPLR	13184	8	7	1.03	8,215,926	10	1.06	8,418,396	10	1.06	1	7,939,271	10	1.07	8,015,276	10	0.98	7,291,690	10	1	7,462,323	10
BCG_0050C	HYPOTHETICAL PROTEIN TB39 8	56003	4	4	0.81	2,093,896	5	0.67	1,723,078	5	1.06	1	2,583,908	5	1	2,434,164	5	0.85	2,071,829	5	1	2,439,383	5
BCG_0200	HYPOTHETICAL PROTEIN TB18 5	17738	2	2	0.84	695,555	4	0.82	680,398	4	1.06	1	826,178	4	0.81	634,784	4	0.79	617,881	4	1	781,024	4
BCG_1453	PUTATIVE S-ADENOSYLMETHIONINE SYNTHETASE MI	43019	2	2	1.35	1,183,039	2	0.86	752,647	2	1.06	1	879,515	2	0.71	592,691	2	0.84	697,315	2	1	833,555	2
BCG_1072C	PUTATIVE 50S RIBOSOMAL PROTEIN L25 RPLY	22441	2	1	0.68	176,176	3	0.73	191,470	3	1.05	1	260,758	3	0.51	126,830	3	0.65	161,810	3	1	249,496	3
BCG_1472C	PUTATIVE LIPOPROTEIN LPRG	24548	3	3	0.91	2,032,290	5	0.88	1,959,113	5	1.04	1	2,229,651	5	0.88	1,869,156	5	0.93	1,980,264	5	1	2,136,484	5
BCG_0716	DNA-DIRECTED RNA POLYMERASE SUBUNIT BETA RF	129236	24	21	1.17	19,140,354	32	0.92	14,935,702	32	1.04	1	16,348,024	32	0.92	14,339,855	32	1.12	17,636,208	32	1	15,699,407	32
BCG_0357C	PUTATIVE GLYCEROPHOSPHORYL DIESTER PHOSPH	28319	4	4	0.91	2,280,258	4	1.09	2,717,779	4	1.04	1	2,497,824	4	1.25	3,008,626	4	1.04	2,503,610	4	1	2,404,472	4
BCG_1813	HYPOTHETICAL PROTEIN	20457	8	8	0.97	4,546,990	8	0.88	4,054,309	8	1.03	1	4,529,471	8	0.84	3,676,553	8	0.82	3,574,559	8	1	4,395,150	8
BCG_2360C	PUTATIVE MOLYBDOPTERIN BIOSYNTHESIS PROTEIN	35271	2	2	1.38	1,333,566	2	1.19	1,151,208	2	1.03	1	965,136	2	1.25	1,170,462	2	1.08	1,016,318	2	1	937,547	2
BCG_2840C	HYPOTHETICAL PROTEIN	25773	2	2	0.91	1,271,738	3	1.15	1,611,893	3	1.01	1	1,400,525	3	1	1,378,834	3	0.94	1,295,193	3	1	1,380,514	3
BCG_1681	50S RIBOSOMAL PROTEIN L35 RPMI	7220	3	2	1.31	2,564,481	6	1.68	3,277,588	6	1.01	1	1,955,825	6	1.53	2,955,155	6	1.09	2,104,019	6	1	1,930,688	6
BCG_0755	PUTATIVE 30S RIBOSOMAL PROTEIN S19 RPSS	10804	13	7	0.99	8,348,383	17	1.27	10,761,256	17	1.00	1	8,477,478	17	1.15	9,738,759	17	1.03	8,715,492	17	1	8,454,342	17
BCG_2962C	PUTATIVE MULTIFUNCTIONAL MYCOCEROSIC ACID S'	224396	5	5	1.37	4,237,806	8	0.84	2,587,265	8	1.00	1	3,084,434	8	0.51	1,574,373	8	1.14	3,492,314	8	1	3,087,421	8
BCG_3453C	HYPOTHETICAL PROTEIN	14317	3	2	0.96	626,270	3	1.05	689,672	3	0.99	1	654,493	3	1.07	706,042	3	1	658,738	3	1	659,899	3
BCG_3052C	PUTATIVE ELECTRON TRANSFER FLAVOPROTEIN (BE	28081	2	2	2.25	1,224,570	3	1.04	565,385	3	0.99	1	543,515	3	0.75	411,708	3	1.25	688,152	3	1	551,441	3
BCG_0084	PUTATIVE 30S RIBOSOMAL PROTEIN S6 RPSF	10935	5	5	0.79	3,151,599	6	0.99	3,943,882	6	0.98	1	4,001,761	6	0.84	3,413,649	6	0.87	3,526,453	6	1	4,070,749	6
BCG_3252	PUTATIVE SHORT-CHAIN DEHYDROGENASE/REDUCT/	29814	2	2	1.39	1,657,685	2	1	1,185,846	2	0.98	1	1,190,836	2	0.94	1,141,262	2	1.27	1,545,314	2	1	1,212,874	2
BCG_2541C	HYPOTHETICAL PROTEIN	8374	2	2	0.71	1,241,151	2	0.94	1,636,893	2	0.96	1	1,748,696	2	0.83	1,496,343	2	0.89	1,616,392	2	1	1,814,618	2
BCG_3863C	PUTATIVE FATTY-ACID-COA LIGASE FADD32	69260	5	4	0.85	2,009,077	6	0.85	1,996,226	6	0.96	1	2,353,165	6	0.96	2,339,840	6	0.94	2,289,701	6	1	2,443,937	6
BCG_3523C	PUTATIVE 30S RIBOSOMAL PROTEIN S4 RPSD	23476	29	21	1.08	18,149,619	38	1.08	18,165,715	38	0.96	1	16,804,360	38	1.12	19,532,495	38	0.89	15,584,058	38	1	17,461,998	38
BCG_0183	PUTATIVE ALDEHYDE DEHYDROGENASE (NAD+) DEPI	55035	6	6	1.07	4,146,828	9	1.68	6,535,578	9	0.96	1	3,863,441	9	1.64	6,615,281	9	1.51	6,103,857	9	1	4,028,901	9
BCG_2911C	PUTATIVE 30S RIBOSOMAL PROTEIN S2 RPSB	31089	11	9	1.09	8,519,527	13	1.06	8,217,342	13	0.96	1	7,806,554	13	1.2	9,853,176	13	1.04	8,562,248	13	1	8,167,493	13
BCG_2235	PUTATIVE TRANSMEMBRANE PROTEIN	26830	8	7	1.39	5,726,577	9	1.78	7,229,363	9	0.95	1	4,107,477	9	1.87	8,012,363	9	1.4	5,942,780	9	1	4,342,837	9
BCG_1682	50S RIBOSOMAL PROTEIN L20 RPLT	14527	6	6	1.5	4,744,640	12	1.41	4,447,438	12	0.94	1	3,162,950	12	1.63	5,475,228	12	1.29	4,317,207	12	1	3,372,448	12
BCG_1324	HYPOTHETICAL PROTEIN	25230	2	2	0.9	442,469	3	0.79	388,482	3	0.93	1	489,736	3	0.94	498,504	3	0.89	467,879	3	1	528,125	3
BCG_0765	PUTATIVE 50S RIBOSOMAL PROTEIN L24 RPLX	11475	4	3	1.05	3,860,189	4	1.06	3,872,761	4	0.92	1	3,657,991	4	0.92	3,670,214	4	0.98	3,883,938	4	1	3,973,630	4
BCG_0767	PUTATIVE 30S RIBOSOMAL PROTEIN S14 RPSN1	6825	2	1	1.13	624,589	4	1.31	722,706	4	0.92	1	550,148	4	1.1	660,156	4	1.09	649,737	4	1	598,284	4
BCG_0717	DNA-DIRECTED RNA POLYMERASE (BETA' CHAIN) RP(	146710	45	40	1.31	34,582,153	61	1.02	26,909,725	61	0.90	1	26,470,689	61	1.02	29,786,012	61	1.19	34,888,297	61	1	29,299,144	61
BCG_0078C	HYPOTHETICAL PROTEIN	20408	2	2	1.11	1,472,087	2	0.93	1,228,938	2	0.90	1	1,322,887	2	1.1	1,619,669	2	0.9	1,318,349	2	1	1,469,306	2
BCG_0391	PUTATIVE CHAPERONE PROTEIN DNAJ1	41315	3	3	0.6	904,448	7	0.87	1,309,512	7	0.89	1	1,508,886	7	0.57	967,202	7	0.7	1,185,596	7	1	1,692,749	7
BCG_0691C	METHOXY MYCOLIC ACID SYNTHASE 4 MMAA4	34636	3	3	0.82	1,923,288	4	0.73	1,720,277	4	0.89	1	2,344,162	4	0.66	1,734,446	4	0.6	1,569,411	4	1	2,632,433	4
BCG_0734	PUTATIVE ELONGATION FACTOR TU TUF (EF-TU)	43594	5	4	1.66	3,198,519	6	1.02	1,983,955	6	0.88	1	1,945,674	6	0.86	1,885,606	6	1.32	2,912,550	6	1	2,202,899	6
BCG_2929C	HYPOTHETICAL PROTEIN	8521	7	5	0.79	1,780,913	10	0.88	1,983,412	10	0.88	1	2,226,202	10	0.69	1,732,148	10	0.67	1,695,910	10	1	2,528,948	10
BCG_0504C	HYPOTHETICAL PROTEIN	21305	3	3	0.73	979,834	4	0.73	973,608	4	0.88	1	1,340,437	4	0.7	1,070,754	4	0.7	1,075,850	4	1	1,530,202	4
BCG_2428	PUTATIVE 30S RIBOSOMAL PROTEIN S20 RPST	9405	8	7	1.58	11,464,267	9	1.56	11,328,324	9	0.86	1	7,198,387	9	1.19	9,990,740	9	1.13	9,462,682	9	1	8,383,780	9
BCG_2462C	PUTATIVE 50S RIBOSOMAL PROTEIN L21 RPLU	11151	7	5	1	5,139,659	8	1.19	6,131,551	8	0.86	1	5,129,042	8	1.09	6,520,674	8	0.93	5,586,592	8	1	5,978,979	8
BCG_1595	PUTATIVE FATTY ACYL-COA REDUCTASE	36821	10	10	0.93	7,890,734	13	1.09	9,231,124	13	0.84	1	8,463,675	13	0.87	8,690,043	13	0.83	8,353,608	13	1	10,036,474	13
BCG_2305	PUTATIVE CDP-DIACYLGLYCEROL PYROPHOSPHATA!	28608	2	2	0.94	1,528,054	3	1.14	1,852,639	3	0.83	1	1,633,024	3	1.18	2,318,161	3	1.18	2,322,601	3	1	1,969,295	3
BCG_0573	HYPOTHETICAL PROTEIN	43055	2	2	0.75	585,472	4	0.77	601,372	4	0.82	1	779,967	4	0.69	653,145	4	0.74	701,244	4	1	946,402	4
BCG_2925C	PUTATIVE 50S RIBOSOMAL PROTEIN L19 RPLS	13013	9	9	0.96	6,759,359	11	0.94	6,604,559	11	0.82	1	7,044,061	11	0.97	8,382,849	11	0.76	6,583,601	11	1	8,638,014	11
BCG_3010	PUTATIVE TRANSCRIPTIONAL REGULATORY PROTEIN	24316	11	10	0.92	3,978,100	14	0.96	4,133,943	14	0.81	1	4,327,570	14	1.01	5,411,983	14	0.84	4,504,670	14	1	5,362,156	14
BCG_3915	PUTATIVE HISTONE-LIKE PROTEIN HNS	13823	4	4	1.53	3,250,199	4	1.34	2,842,714	4	0.81	1	2,130,673	4	0.98	2,583,215	4	0.9	2,372,222	4	1	2,645,507	4
BCG_0835	HYPOTHETICAL PROTEIN	25052	2	2	0.89	824,679	3	1.14	1,050,445	3	0.80	1	924,486	3	0.75	865,636	3	0.68	788,838	3	1	1,154,909	3
BCG_3007C	PUTATIVE DNA-BINDING PROTEIN HU HOMOLOG HUP	21292	12	11	1.13	12,376,605	15	1.13	12,377,556	15	0.80	1	11,035,752	15	0.54	7,315,332	15	1.26	17,173,003	15	1	13,840,170	15
BCG_3526C	PUTATIVE 50S RIBOSOMAL PROTEIN L36 RPMJ	4343	2	2	0.74	1,124,603	3	0.92	1,400,833	3	0.79	1	1,518,340	3	0.65	1,251,885	3	0.6	1,161,730	3	1	1,920,284	3
BCG_3509C	PUTATIVE 50S RIBOSOMAL PROTEIN L13 RPLM	16337	5	5	0.94	3,036,712	7	1.05	3,377,329	7	0.79	1	3,253,703	7	0.79	3,267,399	7	0.87	3,594,451	7	1	4,128,536	7
BCG_3878C	PUTATIVE ACYLTRANSFERASE	28454	4	4	0.97	2,952,341	4	1.12	3,405,096	4	0.79	1	3,048,064	4	0.86	3,337,813	4	0.83	3,215,575	4	1	3,874,980	4
BCG_3487C	60 KDA CHAPERONIN 1 GROEL1	55877	5	5	1.19	4,389,211	7	0.96	3,562,371	7	0.78	1	3,704,160	7	0.58	2,756,237	7	1.02	4,834,698	7	1	4,722,366	7
BCG_2803C	PUTATIVE 30S RIBOSOMAL PROTEIN S15 RPSO	10475	4	4	0.96	2,869,586	5	1.15	3,421,560	5	0.77	1	2,981,864	5	0.71	2,753,425	5	0.9	3,462,667	5	1	3,866,898	5
BCG_2862C	HYPOTHETICAL PROTEIN	19565	5	5	1.02	3,600,629	6	1.26	4,479,819	6	0.76	1	3,531,190	6	1.13	5,239,702	6	0.95	4,382,316	6	1	4,631,432	6
BCG_3488C	10 KDA CHAPERONIN GROES	10804	4	4	1.43	1,433,949	7	6.73	6,734,580	7	0.74	1	1,001,070	7	1.46	1,962,296	7	1.04	1,401,033	7	1	1,348,917	7
BCG_3270C	HYPOTHETICAL PROTEIN	24567	6	6	1.1	5,525,830	6	1.1	5,533,242	6	0.74	1	5,061,741	6	1.16	7,971,083	6	0.95	6,547,180	6	1	6,873,364	6
BCG_0764	PUTATIVE 50S RIBOSOMAL PROTEIN L14 RPLN	13428	5	5	1.15	4,734,734	9	1.1	4,546,263	9	0.73	1	4,132,696	9	0.95	5,384,834	9	0.85	4,827,127	9	1	5,673,893	9
BCG_0752	PUTATIVE 50S RIBOSOMAL PROTEIN L4 RPLD	23743	10	9	1.26	9,508,073	12	1.32	10,018,038	12	0.72	1	7,508,987	12	0.83	8,564,528	12	0.98	10,243,649	12	1	10,418,954	12
BCG_3727	PUTATIVE TRANSMEMBRANE PROTEIN	18919	3	3	1.28	716,477	3	1.2	671,182	3	0.72	1	558,628	3	1.21	937,759	3	1.08	842,475	3	1	777,574	3
BCG_2243	HYPOTHETICAL PROTEIN	56332	3	3	1.17	1,306,009	6	1.16	1,297,125	6	0.70	1	1,119,628	6	1.26	2,028,633	6	1.12	1,797,137	6	1	1,608,849	6
BCG_0479	60 KDA CHAPERONIN 2 GROEL2	56727	23	20	2.3	34,886,269	29	1.4	21,269,569	29	0.69	1	15,192,740	29	0.72	15,945,987	29	1.56	34,444,710	29	1	21,996,057	29
BCG_0027C	PUTATIVE TRANSMEMBRANE PROTEIN	40944	2	2	1.4	1,366,098	3	1.49	1,450,130	3	0.68	1	974,671	3	1.17	1,688,605	3	1.02	1,465,252	3	1	1,443,710	3
BCG_2649	PUTATIVE METHYLTRANSFERASE	29542	6	6	0.86	3,696,850	11	1.01	4,298,886	11	0.67	1	4,289,676	11	0.76	4,833,424	11	0.58	3,672,613	11	1	6,438,136	11
BCG_0861	PUTATIVE PHOSPHORIBOSYLFORMYLGLYCINAMIDINI	38393	2	2	0.86	760,109	2	0.87	767,784	2	0.66	1	884,890	2	0.81	1,078,233	2	0.98	1,313,762	2	1	1,339,602	2
BCG_1504C	HYPOTHETICAL PROTEIN	18316	2	2	0.85	1,106,654	2	0.94	1,223,425	2	0.64	1	1,296,072	2	0.63	1,259,979	2	0.51	1,028,788	2	1	2,011,858	2
BCG_3127C	PUTATIVE CELL DIVISION ATP-BINDING PROTEIN FTSI	25596	5	5	0.83	1,945,879	10	1.07	2,511,679	10	0.64	1	2,357,143	10	0.72	2,666,550	10	0.81	2,980,963	10	1	3,705,012	10
BCG_1951C	PUTATIVE OXIDOREDUCTASE FADB5	35755	4	4	0.87	2,582,983	4	0.9	2,676,188	4	0.64	1	2,979,720	4	0.67	3,163,053	4	0.79	3,702,759	4	1	4,692,271	4
BCG_2958	PUTATIVE DAUNORUBICIN-DIM-TRANSPORT ATP-BINI	35796	3	3	1.15	1,312,545	3	1.59	1,811,253	3	0.63	1	1,136,130	3	1.1	1,968,305	3	0.95	1,711,695	3	1	1,795,083	3
BCG_0750	30S RIBOSOMAL PROTEIN S10 RPSJ (TRANSCRIPTION	11431	7	6	0.97	4,810,428	9	0.91	4,534,791	9	0.62	1	4,991,378	9	0.65	5,299,195	9	0.64	5,149,920	9	1	8,074,586	9
BCG_0121	HYPOTHETICAL PROTEIN	24649	2	2	0.83	967,831	4	1.37	1,601,897	4	0.62	1	1,166,566	4	0.68	1,292,296	4	0.7	1,322,451	4	1	1,895,484	4
BCG_3978C	HYPOTHETICAL PROTEIN SIMILAR TO JAG PROTEIN	20589	4	3	0.94	1,932,475	4	0.82	1,684,790	4	0.61	1	2,050,882	4	0.59	1,957,373	4	0.78	2,601,765	4	1	3,338,335	4
BCG_0772	PUTATIVE 50S RIBOSOMAL PROTEIN L30 RPMD	7347	2	2	0.93	908,081	3	0.86	840,822	3	0.61	1	975,386	3	0.56	895,607	3	0.52	830,897	3	1	1,591,185	3
BCG_1680	PUTATIVE INITIATION FACTOR IF-3 INFC	22349	3	3	0.89	1,180,326	5	1.2	1,602,971	5	0.61	1	1,331,702	5	0.75	1,641,216	5	0.75	1,628,107	5	1	2,176,508	5
BCG_0280C	PUTATIVE 3-OXOACYL-ACYL-CARRIER PROTEIN] RED	46830	5	4	1.28	3,227,141	8	1.26	3,186,302	8	0.60	1	2,506,473	8	0.78	3,237,257	8	1	4,169,147	8	1	4,153,488	8
BCG_1890C	PUTATIVE NADH DEHYDROGENASE NDH	49718	3	3	1.38	2,629,029	4	1.67	3,194,113	4	0.60	1	1,907,776	4	1.05	3,341,014	4	0.88	2,809,656	4	1	3,192,803	4
BCG_3876C	PUTATIVE ACYLTRANSFERASE	29291	4	4	1.1	3,697,610	6	1.04	3,488,150	6	0.59	1	3,351,119	6	0.82	4,646,203	6	0.84	4,783,091	6	1	5,700,220	6
BCG_3269C	PUTATIVE PREPROTEIN TRANSLOCASE SUBUNIT 1 SE	106022	3	3	1.05	1,396,371	5	1.06	1,411,621	5	0.59	1	1,326,419	5	0.85	1,925,390	5	0.86	1,939,686	5	1	2,265,989	5
BCG_1179C	HYPOTHETICAL PROTEIN	32190	2	2	1	552,992	3	1.1	603,883	3	0.58	1	550,646	3	0.65	614,718	3	0.54	511,515	3	1	943,630	3
BCG_0771	PUTATIVE 30S RIBOSOMAL PROTEIN S5 RPSE	22888	6	6	1.65	2,859,676	9	2.41	4,156,281	9	0.58	1	1,750,805	9	1.18	3,581,093	9	1.11	3,365,213	9	1	3,032,802	9
BCG_2974	HYPOTHETICAL PROTEIN	45104	4	3	1.19	1,403,035	5	0.84	994,895	5	0.54	1	1,178,584	5	0.53	1,145,372	5	0.57	1,243,356	5	1	2,167,756	5
BCG_1908C	PUTATIVE L-LACTATE DEHYDROGENASE (CYTOCHRC	45328	9	9	1.07	4,502,537	10	1.73	7,237,541	10	0.53	1	4,145,299	10	0.98	7,567,122	10	1.32	10,275,346	10	1	7,792,973	10
BCG_3913	HYPOTHETICAL PROTEIN	23811	5	5	1.13	3,408,373	9	1.57	4,733,018	9	0.52	1	3,023,360	9	0.84	4,825,267	9	1.24	7,130,497	9	1	5,767,262	9
BCG_2973	PUTATIVE METHYLTRANSFERASE	30652	3	3	0.95	978,829	6	0.91	941,367	6	0.51	1	1,036,669	6	0.73	1,480,241	6	0.64	1,290,752	6	1	2,032,832	6
BCG_3662C	PUTATIVE LSR2 PROTEIN PRECURSOR	12098	7	5	1.31	2,573,265	10	1.08	2,134,221	10	0.50	1	1,967,415	10	0.95	3,767,984	10	1.2	4,777,720	10	1	3,948,870	10
BCG_0086	PUTATIVE 30S RIBOSOMAL PROTEIN S18-1 RPSR1	9543	14	11	1.35	8,195,270	16	1.89	11,282,673	16	0.46	1	6,001,012	16	0.84	10,875,689	16	0.99	12,977,724	16	1	13,159,809	16
HA-UBIQUITIN	HA-Ubiquitin	21912	2	2	2.12	3,434,181	2	1.22	1,983,173	2	0.45	1	1,619,674	2	0.61	2,206,831	2	0.72	2,569,189	2	1	3,595,275	2
BCG_0756	PUTATIVE 50S RIBOSOMAL PROTEIN L22 RPLV	20380	3	3	3.11	3,556,369	3	3.25	3,711,455	3	0.37	1	1,143,427	3	0.96	2,930,862	3	1.22	3,749,139	3	1	3,062,827	3
BCG_0087	PUTATIVE 50S RIBOSOMAL PROTEIN L9 RPLI	16170	3	3	1.11	1,902,294	3	0.75	1,283,335	3	0.36	1	1,707,307	3	0.49	2,321,494	3	0.72	3,436,850	3	1	4,754,484	3
BCG_0683	PUTATIVE 50S RIBOSOMAL PROTEIN L33 RPMG2	6496	3	2	1.04	2,825,605	3	0.98	2,653,806	3	0.36	1	2,713,552	3	0.45	3,433,231	3	0.53	4,039,461	3	1	7,567,669	3
BCG_0813C	PUTATIVE ZINC-CONTAINING ALCOHOL DEHYDROGEI	39748	2	1	1.12	256,878	2	0.83	190,942	2	0.21	1	229,802	2	1.06	1,144,450	2	1.07	1,150,563	2	1	1,078,172	2

Supplementary Table 3:
6-plexed Chemoproteomics Experiment #3

Name	Protein description	MW	no_of_Quant. Spectra	no_of_Quant. Uniq. Peptides	IC50 (μM)	Hill Slope
BCG_0957	PUTATIVE ENOYL-COA HYDRATASE ECHA6	26029	73	21	1.81	0.93
BCG_0023C	PUTATIVE CHROMOSOME PARTITIONING PROT	37018	2	2	>30	
BCG_0027C	PUTATIVE TRANSMEMBRANE PROTEIN	40944	2	2	>30	
BCG_0050C	HYPOTHETICAL PROTEIN TB39 8	56003	2	2	>30	
BCG_0085	PUTATIVE SINGLE-STRAND BINDING PROTEIN S	17353	38	7	>30	
BCG_0086	PUTATIVE 30S RIBOSOMAL PROTEIN S18-1 RPS	9543	4	3	>30	
BCG_0389	PUTATIVE CHAPERONE PROTEIN DNAK	66831	6	6	>30	
BCG_0437C	PUTATIVE ACYL-COA DEHYDROGENASE FADE7	42297	4	4	>30	
BCG_0479	60 KDA CHAPERONIN 2 GROEL2	56727	12	12	>30	
BCG_0504C	HYPOTHETICAL PROTEIN	21305	3	3	>30	
BCG_0516	HEPARIN BINDING HEMAGGLUTININ HBHA	21534	10	9	>30	
BCG_0573	HYPOTHETICAL PROTEIN	43055	3	3	>30	
BCG_0590C	HYPOTHETICAL PROTEIN	14346	2	2	>30	
BCG_0691C	METHOXY MYCOLIC ACID SYNTHASE 4 MMAA4	34636	3	3	>30	
BCG_0716	DNA-DIRECTED RNA POLYMERASE SUBUNIT BE	129236	18	14	>30	
BCG_0717	DNA-DIRECTED RNA POLYMERASE (BETA' CHAI	146710	16	16	>30	
BCG_0734	PUTATIVE ELONGATION FACTOR TU TUF (EF-TU	43594	6	5	>30	
BCG_0750	30S RIBOSOMAL PROTEIN S10 RPSJ (TRANSCRI	11431	4	4	>30	
BCG_0755	PUTATIVE 30S RIBOSOMAL PROTEIN S19 RPSS	10804	2	1	>30	
BCG_0757	PUTATIVE 30S RIBOSOMAL PROTEIN S3 RPSC	30020	9	8	>30	
BCG_0767	PUTATIVE 30S RIBOSOMAL PROTEIN S14 RPSN:	6825	2	1	>30	
BCG_0770	PUTATIVE 50S RIBOSOMAL PROTEIN L18 RPLR	13184	3	3	>30	
BCG_0780	HYPOTHETICAL PROTEIN	25980	5	5	>30	
BCG_0956C	PUTATIVE ACETYL-COENZYME A CARBOXYLASI	51772	9	9	>30	
BCG_0963	HYPOTHETICAL PROTEIN	27627	3	3	>30	
BCG_1463	PUTATIVE PRIMOSOMAL PROTEIN N' PRIA	69839	4	4	>30	
BCG_1472C	PUTATIVE LIPOPROTEIN LPRG	24548	2	2	>30	
BCG_1595	PUTATIVE FATTY ACYL-COA REDUCTASE	36821	7	7	>30	
BCG_1668	PUTATIVE RIBOSOMAL PROTEIN S1 RPSA	53232	4	4	>30	
BCG_1676	EXCINUCLEASE ABC, SUBUNIT A UVRA	106132	4	4	>30	
BCG_1798	PUTATIVE CUTINASE CUT1	21999	2	1	>30	
BCG_1812C	HYPOTHETICAL INTEGRAL MEMBRANE PROTEII	63512	12	12	>30	
BCG_2142	HYPOTHETICAL PROTEIN	31871	9	6	>30	
BCG_2299	PUTATIVE ESTERASE LIPM	46681	2	2	>30	
BCG_2314	HYPOTHETICAL PROTEIN	34986	2	2	>30	
BCG_2447	ALKYL HYDROPEROXIDE REDUCTASE C PROTE	21566	7	6	>30	
BCG_2607C	ADENINE PHOSPHORIBOSYLTRANSFERASE AP	23246	2	2	>30	
BCG_2616C	PUTATIVE HOLLIDAY JUNCTION DNA HELICASE	20189	7	7	>30	
BCG_2724	IRON-DEPENDENT REPRESSOR AND ACTIVATO	25233	2	2	>30	
BCG_2767	HYPOTHETICAL PROTEIN	33610	2	2	>30	
BCG_2801C	BIFUNCTIONAL PROTEIN POLYRIBONUCLEOTID	79735	18	16	>30	
BCG_2859C	PUTATIVE TRANSLATION INITIATION FACTOR IF	94041	3	3	>30	
BCG_2925C	PUTATIVE 50S RIBOSOMAL PROTEIN L19 RPLS	13013	2	2	>30	
BCG_3007C	PUTATIVE DNA-BINDING PROTEIN HU HOMOLO	21292	6	5	>30	
BCG_3008C	PUTATIVE 3-ISOPROPYLMALATE DEHYDRATASE	21780	2	2	>30	
BCG_3009C	PUTATIVE 3-ISOPROPYLMALATE DEHYDRATASE	50199	4	4	>30	
BCG_3142	PUTATIVE THIOSULFATE SULFURTRANSFERASI	35999	4	4	>30	
BCG_3222C	PUTATIVE DNA HELICASE II HOMOLOG UVRD2	75604	14	13	>30	
BCG_3277C	PUTATIVE ADENOSYLHOMOCYSTEINASE SAHH	54324	3	3	>30	
BCG_3487C	60 KDA CHAPERONIN 1 GROEL1	55877	2	2	>30	
BCG_3488C	10 KDA CHAPERONIN GROES	10804	2	2	>30	
BCG_3521C	PUTATIVE 50S RIBOSOMAL PROTEIN L17 RPLQ	19475	2	2	>30	
BCG_3522C	PUTATIVE DNA-DIRECTED RNA POLYMERASE (A	37706	9	8	>30	
BCG_3523C	PUTATIVE 30S RIBOSOMAL PROTEIN S4 RPSD	23476	8	8	>30	
BCG_3524C	PUTATIVE 30S RIBOSOMAL PROTEIN S11 RPSK	14771	6	5	>30	
BCG_3662C	PUTATIVE LSR2 PROTEIN PRECURSOR	12098	4	4	>30	
BCG_3704C	DNA TOPOISOMERASE I TOPA	102370	45	40	>30	
BCG_3743	PUTATIVE LYASE	37641	2	2	>30	
BCG_3863C	PUTATIVE FATTY-ACID-COA LIGASE FADD32	69260	5	5	>30	
BCG_3904	PUTATIVE BACTERIOFERRITIN BFRB	20442	2	2	>30	
BCG_3915	PUTATIVE HISTONE-LIKE PROTEIN HNS	13823	3	3	>30	

Ligand	K_d (µM)		B_{max}	R^2
C_4-CoA	10.4 ± 2.4		3476 ± 175	0.921
C_{12}-CoA	3.0 ± 1.1		2759 ± 135	0.87
C_{14}-CoA	3.1 ± 0.9		2916 ± 97	0.935
C_{16}-CoA	2.8 ± 1.4		2321 ± 136	0.819
C_{18}-CoA	1.4 ± 1.3		2971 ± 203	0.777
C_{20}-CoA	3.5 ± 0.4		2222 ± 199	0.671
GSK951A	0.45 ± 0.06		169 ± 2	0.957
GSK366A	5.6 ± 0.9		1947 ± 108	0.954
GSK059A	9.6 ± 1.9		2653 ± 240	0.937
GSK572A	1.9 ± 0.6		2506 ± 156	0.837
GSK573A	285.8 ± 68.9		21827 ± 4074	0.980
Competition C_{20}-CoA with GSK951A		**Fold increase of K_d relative to no drug**		
0.25 µM drug	2.6 ± 0.9	0.7	2278 ± 104	0.92
2.5 µM drug	13.6 ± 2.1	3.8	994 ± 52	0.968
10 µM drug	10.2 ± 5.5	2.9	917 ± 144	0.709
Competition C_4-CoA with GSK951A				
0.25 µM drug	8.9 ± 2.7	0.86	4665 ± 381	0.887
2.5 µM drug	23.1 ± 2.8	2.2	3154 ± 162	0.985
10 µM drug	N.D.	-	N.D.	
Binding of point mutant				
$EchA6^{W133A}$ + GSK951A	N.D.	-	N.D.	
$EchA6^{W133A}$ + C_{20}-CoA	141.7 ± 15.3	-	1196 ± 67	0.951

N.D. – not determined due to failure of non-linear fitting.

X-ray diffraction data							
	apo EchA6	EchA6:C20-CoA	EchA6:GSK366	EchA6:GSK059	EchA6:GSK572	EchA6:GSK951	EchA6:GSK729
PDB accession code	5DTP	5DTW	5DU4	5DU6	5DU8	5DUC	5DUF
X-ray source	Diamond I04	Diamond I03	Diamond I04-1	Diamond I03	Diamond I03	In-house	Diamond I04-1
Wavelength (Å)	0.9795	0.9763	0.92	0.9763	0.9762	1.5414	0.92
Space group	$P3_221$	$P2_1$	$H3$	$P2_12_12_1$	$P2_12_12_1$	$P2_12_12_1$	$P6_3$
Cell parameters *a,b,c* (Å)	103.1, 103.1, 143.4	113.7, 51.4, 156.9, β = 106.7º	94.83, 94.83, 87.51	51.4, 116.6, 171.8	51.4, 116, 171.5	51.4, 119.2, 171.6	103.9, 103.9, 54.4
Molecules in asymmetric unit	3	6	1	3	3	3	1
Resolution (last shell) (Å)	89.3 - 1.91 (1.96 - 1.91)	108.9 - 2.4 (2.46 - 2.40)	47.4 - 1.7 (1.75 - 1.70)	85.9 - 2.61 (2.68 - 2.61)	96.1 - 2.23 (2.29 - 2.23)	48.9 - 2.7 (2.85 - 2.70)	51.9 - 1.43 (1.47 - 1.43)
*R*merge (%)[1)]	6.5 (70.4)	8.4 (49.9)	6.4 (53.0)	10.5 (59.2)	9.4 (67.4)	9.8 (35.9)	4.5 (67.5)
Total/unique observations	505752 / 68929	246225 / 68420	175974 / 31804	135533 / 31967	322214 / 50922	338678 / 29564	696415 / 61860
$I/\sigma(I)$ [1)]	15.9 (2.7)	9.6 (2.1)	12.6 (2.7)	8.7 (2.0)	11.9 (2.9)	25.8 (7.3)	26.2 (3.5)
Completeness (%)[1)]	100 (100)	99.4 (99.5)	98.9 (99.3)	99.0 (99.4)	99.9 (99.8)	99.6 (97.5)	100 (99.9)
Multiplicity[1)]	7.3 (7.4)	3.6 (3.3)	5.5 (5.7)	4.2 (4.3)	6.3 (6.2)	11.5 (11.1)	11.3 (11.1)
Refinement							
Resolution range	89.3 - 1.91	108.93 - 2.4	47.4 - 1.7	85.9 - 2.6	96.07 - 2.23	48.9 - 2.7	51.9 – 1.50
Unique reflections	65376	64285	31794	31907	48273	29498	53631
Rcryst / Rfree (%)	18.2 / 20.1	23.7 / 27.6	19.3 / 21.5	19.3 / 24.0	21.9 / 25.4	18.7 / 23.4	17.3 / 18.4
No of non-hydogen atoms	5610	11052	1927	5608	5606	5729	2096
Protein / Ligand / Solvent	5284 / - / 326	10793 / 138 / 121	1800 / 33 / 94	5419 / 87 / 102	5344 / 96 / 163	5452 / 168 / 109	1801 / 24 / 271
RMSD bonds / angles (Å / º)	0.006 / 0.976	0.009 / 1.24	0.006 / 1.2	0.009 / 1.13	0.009 / 1.38	0.009 / 1.38	0.006 / 1.14
Wilson B-factor ($Å^2$)	28.4	32.9	30	40.2	31.6	41.6	19.1
Overall average B-factor ($Å^2$)	32.5	31.1	34.5	47.8	40.4	27.6	23.2
Protein / Ligand / Solvent ($Å^2$)	32.5 / - / 33.5	31.2 / 35.4 / 24.2	34.7 / 34.8 / 31.5	47.9 / 49.2 / 36.1	40.4 / 38.5 / 39.7	26.7 / 56.6 / 23.7	21.7 / 20.6 / 33.4
RMSD B-factors ($Å^2$)	0.95	4.4	1.3	3.2	1.4	3.3	1.9
Ramachandran plot[2)] Favoured / allowed / disallowed (%)	97.4 / 2.5/ 0.1	96.7 / 3.6 / 0.1	97.1 / 2.9 / 0	95.8 / 4.0 / 0.2	96.9 / 3.0 / 0.1	95.6 / 4.4 / 0.0	97.9 / 2.1 / 0

[1)]Values in parentheses refer to the high resolution shell. [2)] The Ramachandran plot distribution was calculated using Molprobity.

	M. tuberculosis H37Rv		*M. bovis* BCG		*M. smegmatis*		*M. marinum*		*M. leprae*	
	% seq id	Accession	% seq id	Accession	% seq id	Accession	% seq id	Accession	% seq id	Accession
EchA6	100	CCP43653.1	100	NP_854586.1	74	YP_889873.1	74	EPQ74024.1	86	NP_302400.1
EchA1[1)]	100	CAB06989.1	-		66	YP_886579.1	92	YP_001848785.1	-	
EchA2	100	CAB09570.1	100	NP_854127.1	-		91	WP_020731738.1	-	
EchA3	100	CAB07121.1	100	NP_854307.1	56	YP_885721.1	85	EPQ73703.1	-	
EchA4	100	CAA17470.1	100	NP_854350.1	90	YP_885774.1	93	YP_001849314.1	-	
EchA5	100	CCP43418.1	100	P_854352.1	82	YP_885776.1	89	WP_020731927.1	-	
EchA7	100	CCP43720.1	100	NP_854653.1	72	YP_889733.1	83	EPQ74105.1	-	
EchA8[1)]	100	CCP43821.1	100	NP_854754.1	82	YP_889523.1	91	YP_001852658.1	86	NP_302555.1
EchA9	100	CCP43822.1	100	NP_854755.1	68	YP_889522.1	83	WP_020729788.1	78	NP_302554.1
EchA10	100	CCP43897.1	100	NP_854830.1	64	YP_889431.1	70	YP_001852570.1	-	
EchA11	100	CCP43896.1	100	NP_854829.1	61	YP_889431.1	61	WP_020729866.1	-	
EchA12	100	CCP44231.1	99	NP_855159.1	82	YP_006567817.1	90	WP_020724991.1	72	NP_301896.1
EchA13	100	CCP44702.1	100	NP_855620.1	62	YP_006570456.1	86	YP_001851158.1	-	-
EchA14	100	CCP45280.1	100	NP_856158.1	75	YP_888969.1	43	YP_001852883.1	-	
EchA15	100	CCP45477.1	100	NP_856344.1	33	YP_889854.1	88	YP_001850341.1	-	
EchA16	100	CCP45632.1	100	YP_978935.1	81	YP_886978.1	90	YP_001850207.1	-	
EchA17	100	CCP45848.1	100	NP_856710.1	67	YP_885445.1	82	WP_020724610.1	86	NP_302187.1
EchA18	100	CCP46194.1	100	NP_857049.1	-		-		-	
EchA19[1)]	100	CCP46338.1	99	NP_857184.1	84	YP_890141.1	91	YP_001853261.1	-	
EchA20	100	CCP46372.1	100	NP_857219.1	88	YP_890227.1	94	WP_020730809.1	-	
EchA21[1)]	100	CCP46603.1	100	NP_857440.1	80	YP_890568.1	90	YP_001853588.1	88	NP_301216.1

[1)] EchA paralogues with conserved catalytic carboxylates required for enoyl-CoA hydratases activity are in bold.

Genes	Primer Sequence (5'-3')	Restriction site
EchA6 F_28a	CATGCATGCATATGATCGGTATCACCCAGGCAGA	NdeI
EchA6 R_28a	CATGCATGAAGCTTTTAAGCCCCTTGGAACTTCG	HindIII
TH_EchA6 F	CATGCATGTCTAGAAATGATCGGTATCACCCAGGC	XbaI
TH_EchA6 R	CATGCATGGGATCCTCAGCCCCTTGGAACTTCG	BamHI
TH_FabH F	ACTCTAGAGATGACGGAGATCGCCACGACC	XbaI
TH_FabH R	ATACGGTACCCGACCCTTCGGCATTCGCACCAC	KpnI
TH_KasA F	ACTCTAGAGGTGAGTCAGCCTTCCACCGC	XbaI
TH_KasA R	ATACGGTACCCGGTAACGCCCGAAGGCAAG	KpnI
TH_KasB F	ACTCTAGAGGTGGGGGTCCCCCCGCTTGC	XbaI
TH_KasB R	ATACGGTACCCGGTACCGTCCGAAGGCGATTGC	KpnI
TH_InhA F	ACTCTAGAGATGACAGGACTGCTGGAC	XbaI
TH_InhA R	ATACGGTACCCGGAGCAATTGGGTGTGCGC	KpnI
TH_MabA F	ACTCTAGAGGTGACTGCCACAGCCAC	XbaI
TH_MabA R	ATACGGTACCCGGTGGCCCATACCCATGCC	KpnI
TH_HadA F	ACTCTAGAGGTGGCGTTGAGCGCAGAC	XbaI
TH_HadA R	ATACGGTACCCGCGCAGCGCCATCAGAAAATCC	KpnI
TH_HadB F	ACTCTAGAGATGGCGCTGCGTGAGTTC	XbaI
TH_HadB R	ATACGGTACCCGCGCTAACTTCGCCGAGGC	KpnI
TH_HadC F	ACTCTAGAGATGGCGCTCAAGACCGATATC	XbaI
TH_HadC R	TAC CCG GGG CGC GGT CCT GAT GAC CTG CCC	SmaI
BCG_0957_LL	TTTTTTTTCCATAAATTGGTCCCATGCCGCCGTAGATTCTC	Van91I
BCG_0957_LR	TTTTTTTTCCATTTCTTGGTCCAGGGCCAGACCGTATTTCG	Van91I
BCG_0957_RL	TTTTTTTTCCATAGATTGGTCAACGACGACGGCGCTATC	Van91I
BCG_0957_RR	TTTTTTTTCCATCTTTTGGTCAGGAACCGTCCCGAGAAG	Van91I
mdRv0905_F	GATCGATCAAGCTTATGATCGGTATCACCCAGGC	HindIII
mdRv0905_R	GATCGATCATCGATTTAAGCCCCTTGGAACTTCG	ClaI
EchA6 F_pVV16	CATGCATGCATATGATCGGTATCACCCAGGCAGA	NdeI
EchA6 R_pVV16	CATGCATGAAGCTTAGCCCCTTGGAACTTCGGCG	HindIII
EchA6 F_pMV261	GATCGATCTGGCCAAGATGATCGGTATCACCCAGGC	MscI
EchA6 R_pMV261	GATCGATCAAGCTTTTAAGCCCCTTGGAACTTCG	HindIII
MmpL3 F_pMV261	GGCTGGAATTCATGTTCGCCTGGTGGGGTCG	EcoRI
MmpL3 R_pMV261	GGCAAGCTTTTAAAGGCGTCCTTCGCGGC	HindIII
EchA6^{W133A} F_SDM	GCCCTGGATAACGCGAGCATCCGCCG	-
EchA6^{W133A} R_SDM	CGGCGGATGCTCGCGTTATCCAGGGC	-